Available online at www.sciencedirect.com
ScienceDirect
Advances in Space Research xxx (2010) xxx–xxx
ADVANCES IN SPACE RESEARCH (a COSPAR publication)
www.elsevier.com/locate/asr

Creation of the new industry-standard space test of laser retroreflectors for the GNSS and LAGEOS

S. Dell'Agnello [a,*], G.O. Delle Monache [a], D.G. Currie [b], R. Vittori [c,d], C. Cantone [a], M. Garattini [a], A. Boni [a], M. Martini [a], C. Lops [a], N. Intaglietta [a], R. Tauraso [e,a], D.A. Arnold [f], M.R. Pearlman [f], G. Bianco [g], S. Zerbini [h], M. Maiello [a], S. Berardi [a], L. Porcelli [a], C.O. Alley [b], J.F. McGarry [i], C. Sciarretta [g], V. Luceri [g], T.W. Zagwodzki [i]

[a] *Laboratori Nazionali di Frascati (LNF) dell'INFN via E. Fermi 40, 00044 Frascati, Rome, Italy*
[b] *University of Maryland (UMD), Department of Physics, John S. Toll Building, Regents Drive, College Park, MD 20742-4111, USA*
[c] *Aeronautica Militare Italiana, Viale dell' Università 4, 00185 Rome, Italy*
[d] *Agenzia Spaziale Italiana (ASI), Viale Liegi 26, 00198 Rome, Italy*
[e] *University of Rome "Tor Vergata", Dipartimento di Matematica, Via della Ricerca Scientifica, 00133 Rome, Italy*
[f] *Harvard-Smithsonian Center for Astrophysics (CfA), 60 Garden Street, Cambridge, MA 02138, USA*
[g] *ASI, Centro di Geodesia Spaziale "G. Colombo" (ASI-CGS), Località Terlecchia, P.O. Box ADP, 75100 Matera, Italy*
[h] *University of Bologna, Department of Physics Sector of Geophysics, Viale Berti Pichat 8, 40127 Bologna, Italy*
[i] *NASA, Goddard Space Flight Center (GSCF), code 694, Greenbelt, MD 20771, USA*

Received 1 March 2010; received in revised form 27 October 2010; accepted 30 October 2010

Abstract

We built a new experimental apparatus (the "Satellite/lunar laser ranging Characterization Facility", SCF) and created a new test procedure (the SCF-Test) to characterize and model the detailed thermal behavior and the optical performance of cube corner laser retroreflectors in space for industrial and scientific applications. The primary goal of these innovative tools is to provide critical design and diagnostic capabilities for Satellites Laser Ranging (SLR) to Galileo and other GNSS (Global Navigation Satellite System) constellations. The capability will allow us to optimize the design of GNSS laser retroreflector payloads to maximize ranging efficiency, to improve signal-to-noise conditions in daylight and to provide pre-launch validation of retroreflector performance under laboratory-simulated space conditions. Implementation of new retroreflector designs being studied will help to improve GNSS orbits, which will then increase the accuracy, stability, and distribution of the International Terrestrial Reference Frame (ITRF), to provide better definition of the *geocenter* (origin) and the *scale* (length unit).

Our key experimental innovation is the concurrent measurement and modeling of the optical Far Field Diffraction Pattern (FFDP) and the temperature distribution of the SLR retroreflector payload under thermal conditions produced with a close-match solar simulator. The apparatus includes infrared cameras for non-invasive thermometry, thermal control and real-time movement of the payload to experimentally simulate satellite orientation on orbit with respect to both solar illumination and laser interrogation beams. These unique capabilities provide experimental validation of the space segment for SLR and Lunar Laser Ranging (LLR).

We used the SCF facility and the SCF-Test to perform a comprehensive, non-invasive space characterization of older generation, back-coated retroreflectors of the GIOVE-A and -B (Galileo In-Orbit Validation Elements) and the GPS-35 and -36 designs. First, using a full GPS flight model at laser wavelengths of 532 and 632 nm, we found its "effective optical cross section" in air, under isothermal conditions, to be six times lower than the *Retroreflector Standard for GNSS satellites* (100×10^6 m^2 at 20,000 km altitude for GPS and 180×10^6 m^2 for Galileo at 23,200 km altitude), issued by the International Laser Ranging Service (ILRS). Under the simulated thermal and space conditions of the SCF, we also showed that in some space configurations the "effective optical cross section" is further reduced, by the thermal degradation of the FFDP. Using the same SCF-Test configuration on an individual GIOVE prototype cube, we

* Corresponding author. Tel.: +39 06 94032730; fax: +39 06 94032475.
E-mail address: Simone.DellAgnello@lnf.infn.it (S. Dell'Agnello).

0273-1177/$36.00 © 2010 COSPAR. Published by Elsevier Ltd. All rights reserved.
doi:10.1016/j.asr.2010.10.022

Please cite this article in press as: Dell'Agnello, S., et al. Creation of the new industry-standard space test of laser retroreflectors for the GNSS and LAGEOS. J. Adv. Space Res. (2010), doi:10.1016/j.asr.2010.10.022

measured severe thermal degradation in optical performance, which appears to be caused by the retroreflector metal coating and the non-optimized thermal conductance of the mounting.

Uncoated retroreflectors with proper mounting can minimize thermal degradation and significantly increase the optical performance, and as such, are emerging as the recommended design for modern GNSS satellites. The COMPASS-M1, GLONASS-115 GNSS satellites use uncoated cubes. They provide better efficiency than those on GPS and GIOVE, including better daylight ranging performance. However, these retroreflectors were not characterized in the laboratory under space conditions prior to launch, so we have no basis to evaluate how well they were optimized for future GNSS satellites. SCF-Testing, under a non-disclosure agreement between INFN-LNF and the European Space Agency (ESA), of prototype uncoated cubes for the first four Galileo satellites to be launched (named "IOV", In-Orbit Validation satellites) is a major step forward. An SCF-Test performed on a LAGEOS (LAser GEOdynamics Satellite) engineering model retroreflector array provided by NASA, showed the good space performance on what is now a reference ILRS payload standard. The IOV and LAGEOS measurements demonstrated the effectiveness of the SCF-Test as an LRA diagnostic, optimization and validation tool in use by NASA, ESA and ASI.
© 2010 COSPAR. Published by Elsevier Ltd. All rights reserved.

Keywords: Galileo; GPS; SLR; New space test; Laser retroreflectors; Industry-standard; LAGEOS

1. Introduction

The ITRF provides the stable coordinate system that allows us to measure change in conditions (link measurements) on the Earth's land, oceans, ice and atmosphere over space, time and evolving technologies. The ITRF is an accurate, stable set of station positions and velocities that provide the foundation for virtually all space-based and ground-based metric observations of the Earth. The ITRF is established and maintained by the global space geodetic networks that include SLR, VLBI (Very Long Baseline Interferometry), GNSS, and DORIS (Doppler Orbitography and Radiopositioning Integrated by Satellite). Network measurements must be precise, continuous, robust, reliable, and geographically distributed (worldwide). Network measurements are interconnected by co-location of different observing techniques through very carefully determined inter-technique survey vectors.

The ITRF is a practical, periodic realization[1] of the International Terrestrial Reference System (ITRS), which is a world spatial reference system co-rotating with the Earth in its diurnal motion in space as defined by the IUGG resolution N. 2 adopted in Vienna in 1991 (Geodesist's Handbook, 1992). The ITRF is maintained by the International Earth rotation and Reference system Service (IERS) (Dick and Richter, 2004), by combining contributions containing the evolution in time of station positions together with full variance matrices, from each of the ground-based space geodetic measurement techniques: IVS (International VLBI Service, Schlüter and Behrend, 2007), ILRS (Pearlman and Degnan, 2002), IGS (International GNSS Service, Dow et al., 2009), IDS (International DORIS Service, Willis et al., 2010); see Weber and Springer (2001), Willis et al. (1999). The tracking of GNSS satellites plays not only an integral role on the formulation of the ITRF, but it is also the means by which the ITRF is distributed globally so that users worldwide can link their measurements into the Reference Frame.

SLR and LLR are time-of-flight (ToF) measurements with short laser pulses fired from ground stations to orbiting payloads with cube corner retroreflectors (CCRs) for positioning metrology in space. The international laser ranging activity is coordinated by the ILRS under the International Association of Geodesy (IAG).

The ILRS routinely tracks 25–30 satellites equipped with CCR laser retroreflector arrays (LRAs) from low Earth orbits to the Moon, including GNSS altitudes. The ILRS includes the global tracking network with about 40 stations, Operations and Data Centers, Analysis Centers (ACs) that generate data products including time histories of station positions, precision orbits on retroreflector equipped satellites, Earth rotation parameters, gravity field coefficients in order to support research, including fundamental physics. Two ILRS Combination Centers process and combine the time history products from each AC into ILRS data products for submissions to the IERS for the formulation if the ITRF. Associate Analysis Centers provide other data products for the users.

SLR uniquely defines the origin (the "geocenter") and, together with VLBI, the "scale" of length of the ITRF. Each of the techniques contributing to the ITRF measures a different observable quantity (optical versus radio, range versus range rate, terrestrial versus celestial, etc.) and hence has a different set of systematic errors. Careful combination of these data tries to exploit the strengths of each while mitigating the weaknesses. Major benefit comes from the identification and remedy of systematic errors that would otherwise corrupt the results. SLR is the only optical technique and the only one providing a direct measurement of station-to-satellite ranges. As such, it is relied upon for calibration and validation of other techniques including altimetry and GNSS.

The long-term goal is to define and maintain an ITRF with an accuracy of 1 mm and a stability of 0.1 mm/year over a 10-year period (Plag and Pearlman, 2009), and distribute it worldwide. The main drivers for this requirement are sea surface and ice budget, but many other applications are not far behind. This is a substantial improvement from where we are now and will be quite challenging. However,

[1] ITRF2005, see Altamimi et al., 2007; the latest realization is ITRF2008.

improvements in technology, geographic coverage, and modeling techniques provide potential for significant progress. Validating and improving SLR observations of the GNSS, which is the purpose of our work, is a contribution in the needed direction.

CCRs are commonly made of radiation-resistant grades of fused silica, like the old Suprasil T19 (now called Suprasil 1) and the modern Suprasil 311. LRAs are passive, lightweight, maintenance free, and, if built with suitable thermal design and proper choice of materials, can provide very good optical performance virtually indefinitely. This was historically demonstrated with the LRAs of uncoated CCRs deployed on the surface of the Moon by NASA's Apollo 11, 14 and 15 missions. The Apollo uncoated CCR design and mounting scheme (Bender et al., 1973) was inherited by the LAser GEOdynamics Satellites: LAGEOS, by NASA, in 1976 and LAGEOS-II, by NASA and ASI in 1992. Also LAGEOS CCRs are uncoated. SLR orbital precision on specialized geodetic satellites such as LAGEOS is about 1 cm (RMS of the range residuals). LLR is also achieving cm-level precision (Williams et al., 2006). Since 2007, the new APOLLO station has delivered LLR data with unprecedented, few-mm range precision (Battat et al., 2009), opening the way to a new era in LLR science products and applications.

The first generation GNSS constellations, GLONASS and GPS, deployed fused silica CCR, back-coated with aluminum (Al) starting in the late 1980s. New GNSS constellations and satellites are starting to use uncoated fused silica retroreflectors. Hollow CCRs have been considered but have no flight heritage yet.

In space, CCRs are subjected to strongly varying thermal conditions as their exposure to solar radiation, radiation from the Earth and Moon, and deep space changes. An axial CCR thermal gradient of a few degrees translates linearly into a gradient in the index of refraction, which is $\sim 10^{-5}$/K at 300 K for fused silica. For CCRs with dimensions of a few cm, the *Far Field Diffraction Pattern* (FFDP) is seriously altered, degrading the laser return at the ground. Likewise, the FFDP is extremely sensitive to the detailed mechanical and thermal properties of the structure in which the CCRs are mounted to form an LRA. The CCR thermal behavior is described by CCR *thermal relaxation time* (τ_{CCR}), which is a function of temperature and of other environmental conditions experienced by the LRA on the spacecraft. τ_{CCR} and FFDP are two SLR/LLR *Key Performance Indicators* (KPI) and the main deliverables of the SCF-Test (Section 4).

If the LRA is not a stand-alone test mass like LAGEOS, each CCR may be mounted in a separate cavity, with all cavities mounted on a separate mechanical structure (plate), which is then interfaced to the spacecraft. This is the LRA design used by GLONASS and GPS. This old design is shared also by GIOVE-A and GIOVE-B, launched in 2005 and 2008, and by the first four Galileo satellites that will be launched (the "IOVs"). GIOVE CCRs are aluminum-coated like GLONASS and GPS cubes, while IOV CCRs are uncoated, like the Apollo and LAGEOS cubes. GIOVE and IOV LRAs are described in http://www.ilrs.gsfc.nasa.gov/docs/ESA-EUING-TN-10206_Issue_3.2.pdf. CCRs mounted in single, separate cavities with small mass and heat capacities have a relatively low τ_{CCR}. On the contrary, the Apollo LRAs in the 1960s deployed a different design concept, where a single-body plate of aluminum was machined to obtain cavities into which CCRs were mounted with the lowest possible mount conductance. CCRs mounted into an Al plate of mass and heat capacity larger than for single CCR cavities have a relatively higher value of τ_{CCR}. The first Chinese COMPASS-M1 satellite (Bian et al., 2005), launched in 2007, seems to have an LRA design similar to Apollo (Fumin et al., 2008). For GNSS LRAs are thermally decoupled from the spacecraft to avoid any influence on the critical atomic clocks onboard. The details of any LRA design, the thermal behavior of the cavities, the plate and the spacecraft interface can influence the FFDP. For LLR the CCR FFDP will be sensitive to the type of emplacement structure on the lunar surface, due to the thermal cycle of the regolith (300 K on the surface layer).

Pre-launch SCF-Testing of SLR/LLR payloads will help to diagnose unwanted or unacceptable thermal degradation of their FFDPs and give us an opportunity to improve them with modifications to the design. SCF-Test data will form a database of *effective* thermal and optical characteristics in space conditions (see Section 4) of prototypes, *as-built* flight LRAs or their copies left on the ground.

This paper is organized as follows: Section 2 discusses the motivations and goals for an innovative laboratory characterization of laser retroreflectors under representative space conditions; Section 3 describes the main technical features and operational functionalities of the SCF; Section 4 defines the basic (default) SCF-Test, as well as customized procedures and evolutions of the test; Sections 5 and 6 report the main results of the SCF-Tests to date on a GLONASS/GIOVE CCR prototype and a flight LRA for the GPS; Section 7 discusses the recommended LRA design and SCF validation of modern GNSS constellations; and Section 8 provides the conclusive remarks of the paper.

2. Motivations and goals of the ETRUSCO experiment

Modern GNSS constellations are required to provide improved positioning accuracy, stability and precision with respect to the ITRF. SLR data have been helpful to compare with and validate independently GNSS-only orbits (see Fig. 1). A discussion of the differences and complementary features of the GNSS and SLR techniques, as well as of the advantages of their integration can be found on the ILRS web site (http://ilrs.gsfc.nasa.gov/docs/retroreflector_specification_070416.pdf). The up-to-date *ILRS retroreflector standard* for the effective optical cross section of LRAs at GNSS altitudes is reported in Pearlman (2009) and in Section 6.2.

Please cite this article in press as: Dell'Agnello, S., et al. Creation of the new industry-standard space test of laser retroreflectors for the GNSS and LAGEOS. J. Adv. Space Res. (2010), doi:10.1016/j.asr.2010.10.022

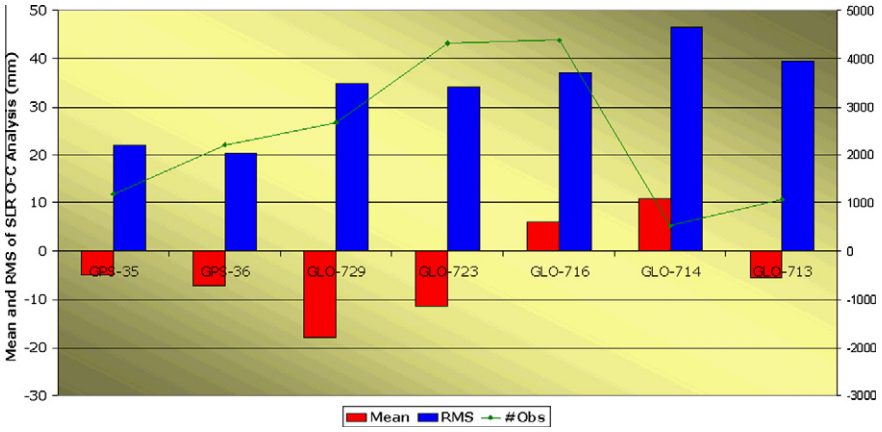

Fig. 1. Residuals of SLR measurements to the computed orbits of GPS and GLONASS satellites equipped with older generation, Al-coated LRAs (courtesy of T. Springer).

LRAs were launched on GPS-35 and -36 in 1993 and 1994, respectively. A third identical array (see Fig. 2), belonging to the University of Maryland, was loaned to LNF and SCF-Tested. The LRAs were also launched on GIOVE-A and -B in 2005 and 2007, respectively. All four LRAs share the traditional GLONASS CCR design, except for their number of CCRs and their geometric footprint. Testing of the third GPS flight array was important because the identical arrays on GPS-35 and -36: (i) do not satisfy the ILRS requirement for LRA effective cross section of GNSS satellites reported in Table 1 and (ii) show weaker performance then anticipated (see Fig. 2). In fact, the GPS and GIOVE arrays should have about the same laser return signal strength, based on their calculated optical cross section, scaled by their different altitudes. On the contrary, the number of returns/s from GIOVE is significantly larger than from GPS LRAs.

With inadequate CCR cross-sections, data is too sparse for the production of viable products, satellite acquisition time increases, and daylight tracking suffers. The long acquisition time reduces the number of satellites that can be tracked, and the lack or difficulty of daylight ranging means that half of the orbit is not tracked. Laser ranging data are available to the user in about 1–2 h after acquisition. In a recent campaign, SLR-only orbits of the GIOVE-A satellite were computed on a weekly basis using the data from the best ILRS stations; the orbital RMS was between 1 and 4 cm (Falcone et al., 2006). In the future, LRAs compliant with the ILRS standard will allow for the production of SLR-only orbits more frequently than weekly and for precise orbit reconstruction of GNSS satellites based on both microwave data and SLR data.

LRAs will be deployed on Galileo, and on future Chinese COMPASS satellites. Activities are underway to try to get retroreflector arrays on the GPS III series. If planned GNSS constellations satellites all carry retroreflector arrays, the total number requiring SLR-tracking could be several dozen. It becomes mandatory to improve LRA performance and satisfy the ILRS standard for GNSS satellites. To address this need, the INFN experiment ETRUSCO (*Extra Terrestrial Ranging to Unified Satellite COnstellation*, 2006–2009) developed the SCF and the SCF-Test to characterize and validate the optical performance of Galileo and other GNSS LRAs under laboratory-simulated space conditions. Retroreflectors on the Galileo satellites will allow us to use SLR to improve and validate their orbits. In addition, improvements in these orbits will improve the Reference Frame and benefit all of the programs that rely on it, includ-

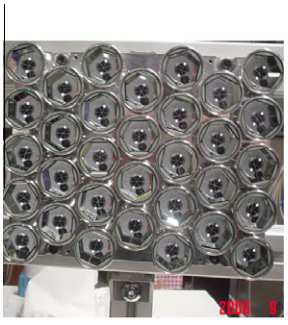

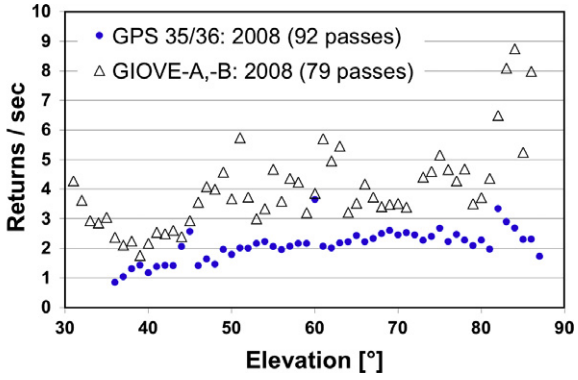

Fig. 2. Left: the third GPS flight CCR array SCF-Tested at LNF. Right: GPS/GIOVE laser returns recorded by the ILRS station at Graz, Austria (courtesy of G. Kirchner).

Please cite this article in press as: Dell'Agnello, S., et al. Creation of the new industry-standard space test of laser retroreflectors for the GNSS and LAGEOS. J. Adv. Space Res. (2010), doi:10.1016/j.asr.2010.10.022

Table 1
Optical cross sections and FFDP thermal degradations of GNSS LRAs.

GNSS satellite	Altitude (10^6 m)	ILRS standard cross section (10^6 m)	Calculated cross section (10^6 m)	Measured cross section in air (10^6 m)	Measured FFDP intensity thermal degradation in SCF-Test conditions (multiplicative factor)
GLONASS	19.1	100	80		0.14 ± 0.02[a]
GPS 35/36	20	100	20	16.4 ± 3.3[b]	0.12 ± 0.02[c]
GIOVE-A and -B	23.9	200	45/40		0.14 ± 0.02[a]

[a] FFDP/SCF-Test of 1 GLONASS proto CCR (2007). Sun: on-axis, intensity = 0.83 × AM0, IR < 3 μm.
[b] FFDP-Test of 32 GPS flight CCRs (early 1990s). Sun: on-axis, intensity = 0.89 × AM0, IR < 3 μm.
[c] SCF-Test of 1 GPS flight CCR (early 1990s). Sun: on-axis, intensity = 0.89 × AM0, IR < 3 μm.

ing payloads on Galileo tracked low Earth-orbiting satellites (altimetry, gravity field, etc.).

3. SCF: the Satellite/lunar laser ranging Characterization Facility

A schematic view of the SCF is shown in Fig. 3. The steel cryostat has a length of about 2 m and a diameter of about 0.9 m. On the right side the cryostat there are three circular ports at 45°, 90° and 135° to its longitudinal axis, available for non-invasive thermal and optical measurements. The inner copper shroud, painted with black Aeroglaze Z306 (0.90 emissivity and low out-gassing), is kept at $T \sim 77$ K with liquid nitrogen. When the shroud is cold, the vacuum reached is in the range of 10^{-6} mbar or better. Two distinct positioning systems at the top of the cryostat (one for roto-translation movements in the plane of the LRA, shown in Fig. 5, and one for spherical rotations and tilts, shown in figure) hold and move the LRA in front of the Solar Simulator (SS), infrared (IR) cameras and laser, all located outside the SCF. Both systems can rotate around the vertical. An Earth infrared Simulator (ES) can be also made available inside the SCF. After SS/ES heating, the LRA inside can be rotated about the vertical axis for laser tests from the 90° port. τ_{CCR} is measured with IR cameras through the 45° and 135° ports equipped with germanium (Ge) windows, during SS/ES heating and FFDP tests. FFDPs can be taken during ES/SS heating through the 45° port (replacing the Ge window with an optical window).

The SS beam enters through the front quartz "AM0" window (37 cm clear diameter, 40 mm thickness), which, aside from Fresnel reflection losses, is transparent to the solar radiation up to about 3 μm. This has been quantified with thermal modeling and validated through auxiliary measurements and calibrations. The effect on the CCRs of IR radiation absorbed for $\lambda > 3$ μm is partly compensated by the IR reemitted by the warm AM0 window and 45°/90°/135° ports. Full compensation is achieved with IR emitters inside the SCF and/or thermal modeling on an LRA-by-LRA basis.

The SS provides a 40 cm diameter beam with close spectral match to the AM0 standard of 1 solar constant in space (1366.1 W/m^2). The spectrum is formed by a metal halide (HMI) arc lamp (UV–Visible; 6 kW), together with a quartz halogen, tungsten filament lamp (Red-IR; 12 kW). The spectra over 400–1800 nm are shown in Fig. 4. The uniformity of the SS intensity is ±5% over 35 cm diameter. The absolute scale of the intensity is maintained by exposing the SS to the *solarimeter*, a standard thermopile (calibrated blackbody), accurate and stable over >5 years to ±2%. During operations, the SS intensity is monitored with a photodiode.

The ES is a disk painted with Aeroglaze Z306, kept at the appropriate temperature and distance to the LRA to provide an IR flux on the LRA comparable to that which would be experienced in space from the Earth IR. Other ES implementations depend on the LRA.

The SCF and its optical table are shown in Fig. 3. The windows on the right side of the cryostat are for the IR cameras, the laser measurements and for spare use. The SS beam enters through the AM0 window. The specifications

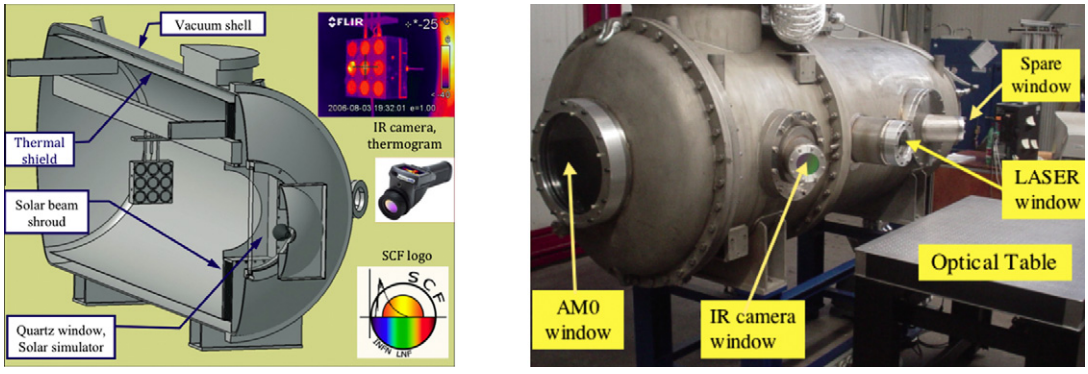

Fig. 3. Left: SCF cryostat with an Apollo/LAGEOS LRA built at LNF (Bosco et al., 2007), LRA thermogram, one IR camera and SCF logo. Right: SCF cryostat, windows and optical table for FFDP tests. The 45° and 135° ports can host windows with clear diameters up to ~ 200 mm.

Please cite this article in press as: Dell'Agnello, S., et al. Creation of the new industry-standard space test of laser retroreflectors for the GNSS and LAGEOS. J. Adv. Space Res. (2010), doi:10.1016/j.asr.2010.10.022

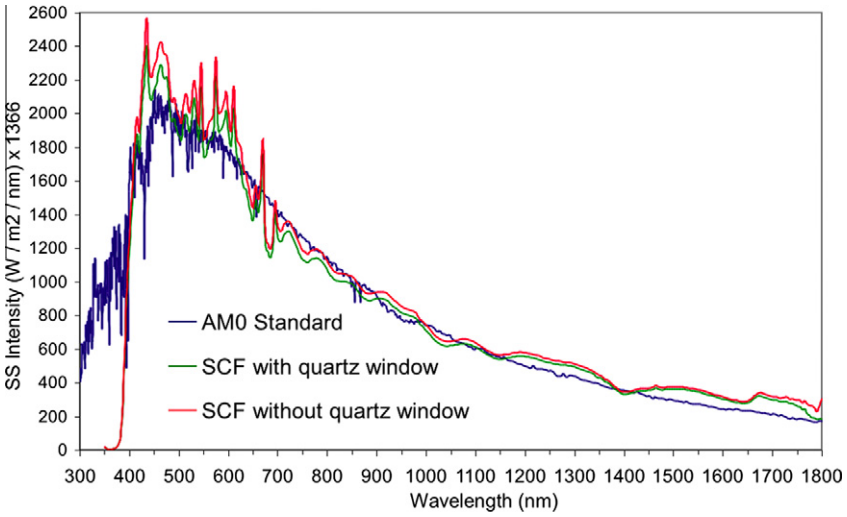

Fig. 4. SS spectra of the SCF with/without quartz window compared to the AM0.

of current LASER window are: fused silica; 120 mm clear and optical aperture, 38 mm thickness, good surface roughness quality (20–10 in scratch–dig units), deformations of the transmitted wavefront $<\lambda/20$, and anti-reflective coating on both sides (reflectivity $\leqslant 0.3\%$ for $\lambda = 532$ and 632.8 nm). On the back of the SCF is another port (not shown in Fig. 3) for other optical, IR camera or AM0 windows. The SCF cryostat and shroud also have numerous other ports distributed on the back, on the bottom, on the left side, with several of them grouped on the top in a large service turret.

CCRs under FFDP test are either in air for isothermal tests, or inside the SCF for tests in representative space conditions (Fig. 5 shows the GPS flight LRA). CCRs are first exposed to the SS and/or ES and then rotated in front of a "LASER" window to acquire its FFDP. Thermograms can be taken from another port (e.g. 45°).

3.1. Temperature measurements and thermal control

The temperature data acquisition system consists of IR cameras for non-invasive, high spatial granularity measurements and class-A PT100 probes with 4-wire readout with standard accuracy and interchangeability of 0.2 K. The PT100s are also used to calibrate the IR cameras. The PT100s temperature scale is checked with a dry-block absolute temperature calibrator capable of $\leqslant 0.1$ K accuracy and with calibrated PT100 systems.

We use different approaches for the thermal control of LRAs in the SCF. To reproduce average conditions in near Earth orbits, we typically control the LRA temperature between to be between 243 and 323 K. For small LRA models we employ thermo-electric coolers (TECs). For flight models (where we need to limit invasive handling) and for models for which we need to provide large heat loads, we use custom-made copper Support and Interface Plates (SIPs) thermally linked to the back of the LRA. These copper plates have molded or brazed copper pipes in which we flow a fluid driven by an external chiller, which allows us to control the LRA temperature between 243 and 423 K. Lower LRA temperatures can be reached by bypassing the external chiller and using the thermal balance between resistive heaters in contact with the copper plate (or the LRA directly) and the cold shroud.

3.2. Optical far field diffraction pattern test

The basic industrial acceptance test of the CCR optical performance is the measurement of the absolute angular size, shape and optical cross section of single-CCR FFDP

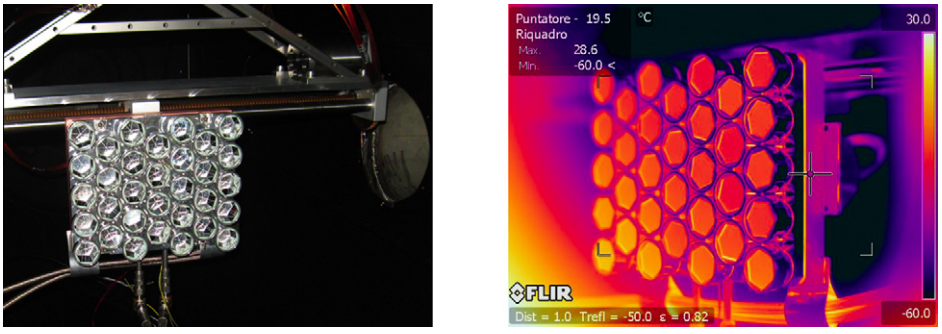

Fig. 5. Third GPS flight array in the SCF. Left: array on the positioning system (which has a horizontal travel of $\pm$ 310 mm) and the LASER window at 90° of the array. Right: IR thermogram taken during SS illumination.

Please cite this article in press as: Dell'Agnello, S., et al. Creation of the new industry-standard space test of laser retroreflectors for the GNSS and LAGEOS. J. Adv. Space Res. (2010), doi:10.1016/j.asr.2010.10.022

with linearly polarized continuous wave lasers (Boni et al., 2008). The horizontal and vertical polarization components of each FFDP are recorded separately. This is particularly important for uncoated CCRs, whose FFDPs depend strongly on the orientation of the input linear polarization. No dependence is expected for coated CCRs. Our laser beam profilers are two 12-bit, 2 Mega-pixel CCD cameras read-out through Firewire or USB with a PC. FFDPs are acquired with the CCR in Air and Isothermal Conditions (AIC). Fig. 6 shows the measured and modeled FFDP of a LAGEOS CCR taken at AIC.

The absolute angular scale of the optical circuit is calibrated with the double-slit method to test the consistency of each CCR FFDP with its nominal Dihedral Angle Offsets (DAO expresses in arcsec or with the symbol ″). The latter are related to the satellite velocity aberration, which is determined by its orbital altitude (velocity). The DAO specifications for the Apollo cubes and the LAGEOS cubes are $0.0'' \pm 0.5''$ and $1.25'' \pm 0.50''$, respectively. The optical specifications of GLONASS/GPS/GIOVE CCRs are given in terms of FFDP intensity at a velocity aberration around 25 μrad. The lack of knowledge of the DAO specifications makes the modeling of the optical FFDP and, especially, its variations due to thermal effects, extremely difficult and unreliable.

FFDP tests were done at two LNF facilities: the Optics Lab with a He–Ne laser (632 nm) and at the SCF with a Nd–Yg laser (532 nm). We also measured the FFDP intensity relative to the Airy Peak, using reference flat mirrors of known reflectivity and good optical quality. From this we extracted the optical cross section, as shown in Section 6.2. FFDP measurements were modeled with CODE V, an optical ray-tracing software package by O.R.A., Inc. The LNF FFDP test procedure was developed in 2007/08 with GLONASS prototypes, the GPS flight LRA and Apollo/LAGEOS CCRs and is described in detail in Boni et al., (2008).

3.3. Apollo/LAGEOS and GLONASS/GPS/GIOVE retroreflectors

The 38.1 mm uncoated Apollo/LAGEOS CCR, its plastic rings of PolyChloroTriFluoroEthylene (KEL-F) and its pristine mounting scheme are shown in Fig. 7. KEL-F was space qualified in the 60s for the Apollo missions. The mounting is a loose fit with axial play between the rings and the CCR tabs of 0.05–0.1 mm. This Apollo mounting was inherited by LAGEOS. Fig. 8 shows the Al-coated CCRs of about 28 mm active diameter used on GLONASS, GPS, GIOVE-A and -B and their mounting. This is significantly more complicated and less thermally insulating than that of Apollo CCRs. This GLONASS-type CCR has a polished Al housing.

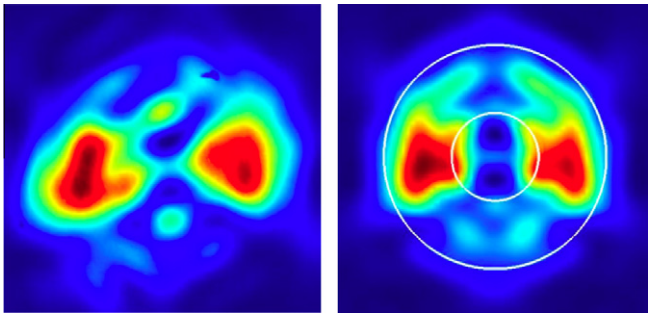

Fig. 6. Measured LAGEOS FFDP (left) and FFDP modeled with DAO ~ 1.25″ (the white circles show the radius of FFDP maxima for DAO = 0.75″ and 1.75″).

3.4. Software modeling suite

Temperature and FFDP data measured at the SCF are modeled with:

- Autodesk Inventor (solid modeling) and ANSYS (FEM analysis).
- For satellite thermal analysis we adopted a specialized suite by C&R-Tech: (i) Thermal Desktop, the CAD-based geometric thermal modeler, (ii) RadCad, the radiation analysis module, and (iii) Sinda-Fluint, the solver and orbital simulator (TRS). TRS can handle satellites with up to about 20,000 FEM nodes and a generic satellite spin and orbit configuration. It also provides the thermal inputs and orbital motions of the Sun, Earth, Moon and other planets of the solar system.
- Optical design and analysis software: CODE V, by O.R.A.

4. SCF-Test: the new industry-standard space test of laser retroreflectors

The SCF-Test consists of the following integrated and concurrent thermal and optical measurements performed on CCR/LRA breadboards, prototypes or flight payloads:

- Hold the average temperature of the CCR/LRA mechanical support structure (Al for Apollo, LAGEOS, GLONASS, GPS, GIOVE, IOV), T_M, to the expected average value, T_{AVG}. In Earth orbits the *default LRA temperature* is $T_{AVG} = 300$ K. T_{AVG}, the expected variation range of T_M and the conditions of the LRA to spacecraft interface are inputs. With SCF data and analysis we evaluate:
  1. CCR FFDPs under simulated space conditions (Fig. 9 right) with the same optical circuit used at the SCF for AIC tests (Fig. 9 left); the laser beam has a *default linear polarization* and an adjustable incidence angle with respect to the normal to the CCR face (the *default laser angle is* 0°);
  2. CCR surface temperature and τ_{CCR};
  3. temperature of components of the LRA other than CCRs.
- Repeat the above for T_M different from T_{AVG}, in the expected variation range.
- Repeat the above for different SS illumination conditions:

Please cite this article in press as: Dell'Agnello, S., et al. Creation of the new industry-standard space test of laser retroreflectors for the GNSS and LAGEOS. J. Adv. Space Res. (2010), doi:10.1016/j.asr.2010.10.022

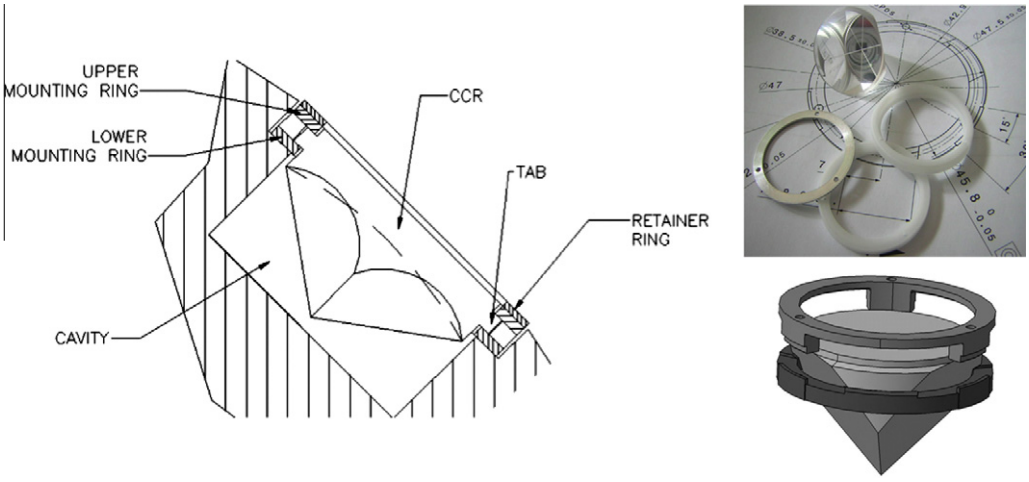

Fig. 7. Apollo/LAGEOS CCR mounting scheme: conceptual drawing of the CCR in the cavity (left, not to scale); photo and drawing of bare CCR, external Al ring and the two internal KEL-F rings (top and bottom right).

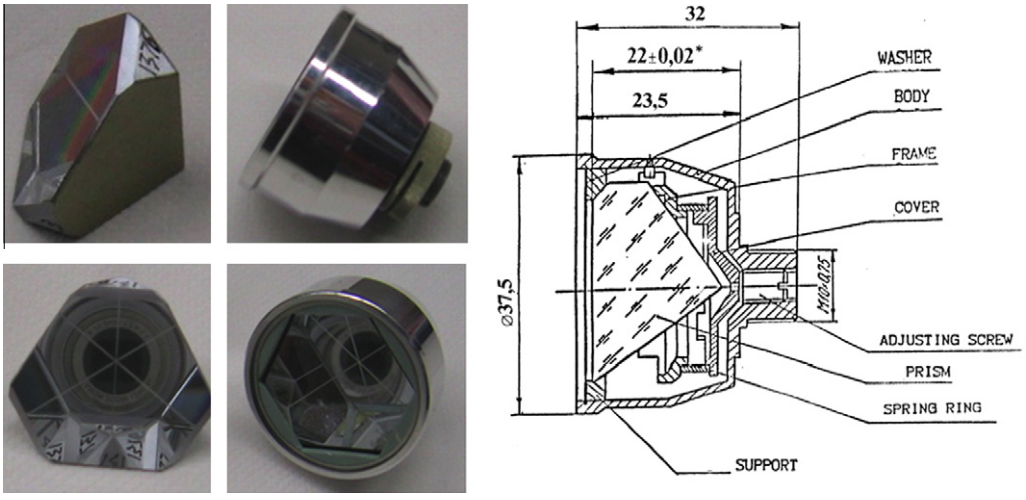

Fig. 8. The GLONASS/GPS/GIOVE CCR: bare coated CCR (left); complete CCR, mounted in its aluminum housing (center); some details of the mounting scheme (right).

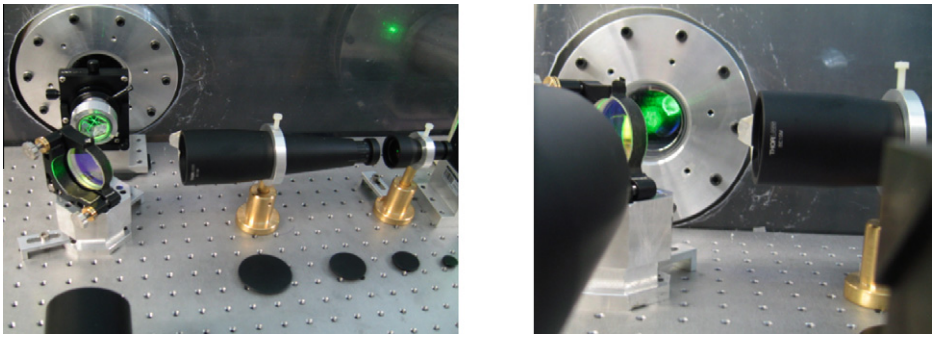

Fig. 9. FFDP measurement of a GLONASS CCR inside the SCF (right) and in air/isothermal conditions (left). The external FFDP optical circuit is the same.

1. transition from SS turned on to off (effect of the Earth shadow or shadow of the spacecraft on the CCR) and vice-versa;
2. different SS illumination angles; the *default SS angle* is 0° with respect to the normal to the CCR face;
3. different times along the CCR thermal relaxation curve.

Please cite this article in press as: Dell'Agnello, S., et al. Creation of the new industry-standard space test of laser retroreflectors for the GNSS and LAGEOS. J. Adv. Space Res. (2010), doi:10.1016/j.asr.2010.10.022

The SCF-Test concept is shown in Fig. 10 for a configuration corresponding to the passage of a satellite equipped with an LRA into the Earth shadow. Customized tests, procedures and experimental setups, not included in the *default SCF-Test* described above, to be defined for specific payloads and applications, include:

- Test *Orthogonal Laser Polarizations* (OLP). This is an SLR/LLR KPI mainly for uncoated solid CCRs, whose FFDP is strongly dependent on the direction of the interrogating linear polarization used by almost all ILRS stations.
- Use LRA orientations with respect to both SS and laser beams in the SCF to simulate and test specific orbit and attitude conditions. In particular, successful SCF-Testing of a Galileo IOV CCR prototype corresponding to a specific Galileo orbit was performed in real-time by ETRUSCO for ESA (see Section 7). This is the ultimate laboratory simulation of LRA space conditions on orbit.
- Measure the τ_{METAL} (thermal relaxation time of LRA metal components).
- Tune the TRS and CODE V models to the SCF data for 'static' climatic conditions, in which the SS and ES are turned on and off alternatively.
- Use validated TRS and CODE V simulations to model the LRA temperature and FFDP transient behavior for specific orbit and attitude conditions, that is, LRA orientations with respect to both solar perturbation and laser interrogation beams.

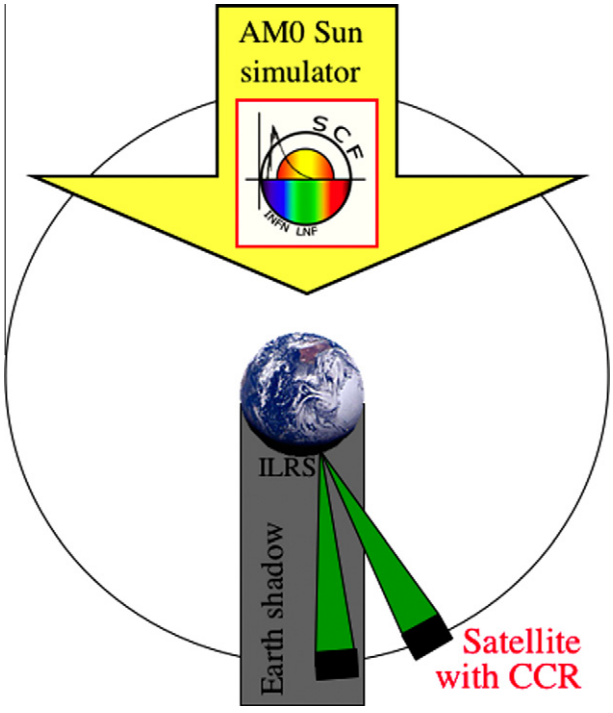

Fig. 10. SCF-Test conceptual drawing.

- Measure the *Wavefront Fizeau Interferogram* (WFI) over the laser beam retroreflected by the CCR. This is an SLR/LLR KPI for all CCR types. This is a new capability being added to the SCF.
- Hold the LRA in the SCF with a thermally insulating support, if needed (for example for stand-alone laser-ranged test-masses like LAGEOS).
- Use different thermal loads for the LRA in planetary orbits or surfaces, or in deep/interplanetary space. SCF-Testing of a new LLR payload (Dell'Agnello et al., 2008) was performed for NASA by LNF with a Co-PI role (NASA Call No. NNH06ZDA001N, Proposal No.: 06-LSSO06-0052).
- Evaluate the temperature difference between the CCR outer face and its corner. The measurement of the corner temperature is difficult both with contact probes (which conduct heat to the corner, becoming potentially unreliable when sunlit by the SS) and with the IR camera (uncertainties related to the IR imaging contrast between the corner and the cavity). Depending on the specific mechanical structure of the LRA, the direct measurement of the corner may not be possible and/or may have to be complemented with TRS modeling. This test is not the correct way of assessing the CCR optical behavior in space, which must be done in a direct way by measuring the FFDP with the SCF-Test. The face-to-corner temperature estimate is only useful to better constrain the LRA modeling.
- Do the SCF-Test after the LRA is exposed to a particle radiation dose relevant to the LRA lifetime in space. This may be needed if the LRA components contain coatings (or heavy elements in the bulk structure) not yet space qualified for the specific LRA application.
- Further testing and TRS customizations upon request.

Default and customized SCF-Testing of a LAGEOS LRA engineering model was performed (see Section 7), since it is the reference SLR payload standard of the ILRS.

Unlike the SCF-Test, incomplete and reduced thermal and/or optical tests of CCRs in vacuum during bulk temperature changes imposed to the LRA without accurate simulation of sun illumination and cold space, without payload thermal control and real-time orbit-like movement/orientation with respect to SS and laser beams do not give reliable information on the space behaviour of the CCR/LRA. Incomplete, reduced testing may give unrealistic and misleading results.

5. Tests of the 2007 GLONASS/GIOVE coated retroreflector prototypes

We describe the FFDP test of three GLONASS CCR prototypes, which were recently manufactured in Russia and provided to LNF in April 2007. One prototype was the standard GLONASS CCR whose external Al housing (i.e. the CCR cavity) had the standard Al polish. This CCR was nominally identical to those deployed on GIO-

Please cite this article in press as: Dell'Agnello, S., et al. Creation of the new industry-standard space test of laser retroreflectors for the GNSS and LAGEOS. J. Adv. Space Res. (2010), doi:10.1016/j.asr.2010.10.022

VE-A and -B. The other two prototypes were coated with different surface materials: a dark grey paint and a white paint. We report the AIC test and then the results of the very first SCF-Test performed on the CCR with the standard polished Al housing. All FFDPs were taken with the laser beam at normal incidence to the surfaces of the three CCRs.

5.1. FFDP tests in air and isothermal conditions at 632 and 532 nm

We measured the FFDP of the three CCRs in AIC at 532 and 632 nm and found them to be consistent with expectations. The FFDP of the GLONASS CCR with polished Al housing measured by the Institute of Precision Instrumentation Engineering (IPIE) in Moscow and by LNF at 532 nm are shown respectively in Fig. 11 (courtesy of V. Vasiliev) and in Fig. 12. The peak-to-peak distance measured by IPIE, about 50 μrad (10 arcsec), agrees with measurements by LNF, about 50 μrad, within our experimental uncertainty of 5–10 μrad including statistical and systematic errors (Boni et al., 2008). This distance corresponds to a 25 μrad velocity aberration, which is taken as the average, nominal value for GNSS altitudes. The two FFDP shapes are also consistent.

The FFDP peak-to-peak distance for the GLONASS CCR with the grey housing measured by LNF and IPIE were, respectively, 49 and 50 μrad. For the CCR with white housing they were 44 and 50 μrad, respectively. FFDP shapes are consistent.

5.2. SCF-Test of one GLONASS/GIOVE retroreflector prototype at 532 nm

The SCF-Test of the polished Al-coated GLONASS prototype CCR was done with simulated space conditions inside the SCF (vacuum $= 10^{-6}$ mbar, cold inner black shroud at ~80 K) and with the Al base (a circular plate) for the CCR support (see below) held fixed at 300 K with a TEC. Once the CCR and its mounting reached thermal equilibrium in the SCF environment (at 284 and 300 K, respectively), we turned on the SS beam at a slightly reduced intensity of about $(0.83 \pm 0.05) \times$ AM0. The solar beam was normally incident to the CCR surface for about 8500 s. The CCR was fixed on an Al cylindrical housing (see inset of Fig. 13). The bottom plate of the housing simulated the LRA Al plate of GLONASS/GPS arrays. The cylindrical Al housing around the CCR (covered by Al paper) simulated the presence of other Al CCRs that would have been present in a full array. Fig. 13 shows the CCR inside the SCF, with its housing attached to a rotation + tilt positioning system which can hold a larger planar or spherical array.

The temperature of the CCR in the heating phase was measured with the IR camera. The CCR was then rotated by 90° within a few seconds, the SS was turned off during the rotation, and CCR FFDPs were recorded at a ~7 Hz rate through the LASER window of the SCF. The CCR warmed up and cooled down with a similar exponential τ_{CCR} (see Fig. 14). When the CCR was hot there were thermal gradients across its body, between the outer surface and the corner inside its Al housing. We looked at FFDPs to see how the optical performance was affected by this thermal gradient transient condition.

We took FFDP movies at 7 Hz for a little less than 2 h and towards the end of this time we took single shots of FFDPs only every 5 min because the FFDP had become stable. Two CCR FFDPs, one taken right after rotation (and turning off the SS) and one taken when the CCR temperature had cooled and become stationary (after the SS had been turned off for 5500 s), are shown in Fig. 15. After these 5500 s, the distance between the two FFDP lobes was the same as that measured in air, when the CCR was isothermal and the lobes where separated by ~50 μrad (see previous section).

When the CCR was hot, the distance between the intensity peaks doubled to about 100 μrad and the intensity of the peaks were reduced to half the 'cold' intensity. That is, the hot CCR retroreflected most of the energy to the wrong angle. If this condition and configuration occurred in GNSS orbit, the signal returned to the ground station

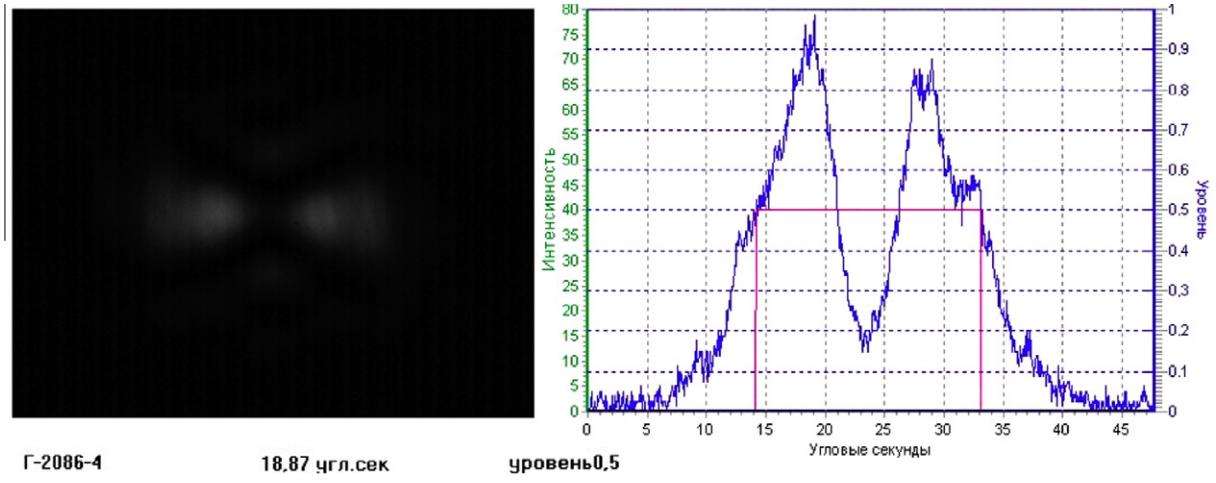

Fig. 11. FFDP angular distance measured by IPIE in arc-sec for 532 nm.

Please cite this article in press as: Dell'Agnello, S., et al. Creation of the new industry-standard space test of laser retroreflectors for the GNSS and LAGEOS. J. Adv. Space Res. (2010), doi:10.1016/j.asr.2010.10.022

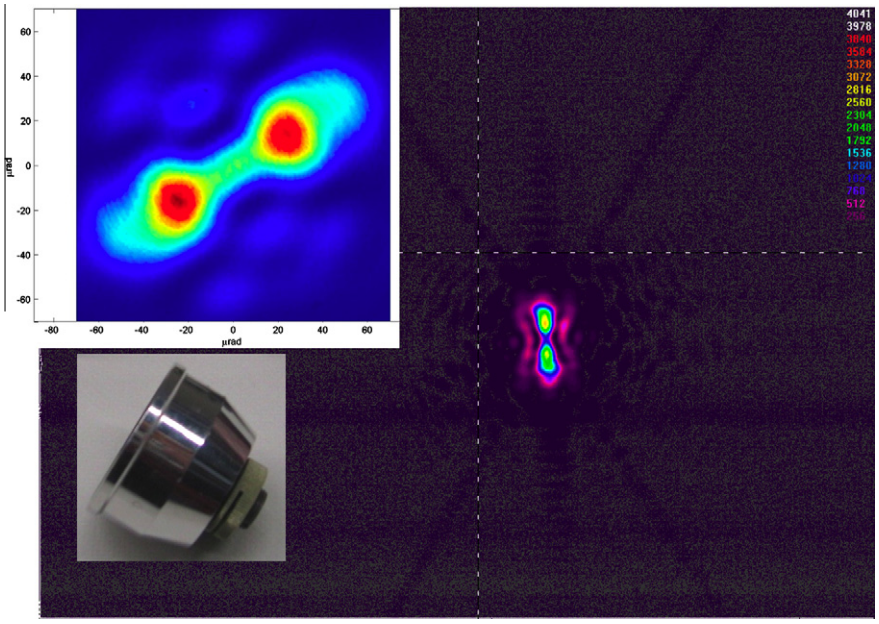

Fig. 12. Al CCR FFDP measured by INFN-LNF at 532 nm (full CCD). The insets on the left show: CCR and its FFDP taken at 632 nm, but with a different CCR orientation.

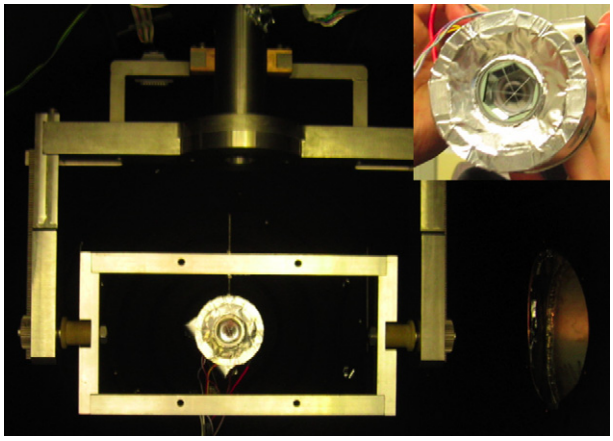

Fig. 13. GLONASS/GIOVE CCR in the SCF. The inset is a blow-up of the CCR. The positioning system does 0–360° rotations and tilts.

would be severely attenuated from the anticipated value (see the next section for further discussion). Figs. 16 and 17 show the variation of the FFDP peak distance and intensities vs. time during the cool-down period.

Data clearly indicates the presence of at least two very different time constants in Figs. 16 and 17: a fast decay (rise) in about a couple of minutes, followed by a thermal recovery of the nominal performance, with a longer time of about 45 min. This second effect seems to change slope at around 1200–1400 s. This is more severe than the fast transient because it affects the FFDP for a longer time.

Our current physical interpretation of the effect of solar radiation in coated CCRs is the following. The front face has a high emissivity. The amount of heat radiated from the front face is proportional to the fourth power of its temperature. The temperature gradient depends on where the heat is coming from. When there is solar radiation there is a large heat input absorbed by the 10 μm metal coatings on the back of the cube. This has to be conducted along a long path length through the CCR to its front face. This creates a large thermal gradient. There is also heat coming

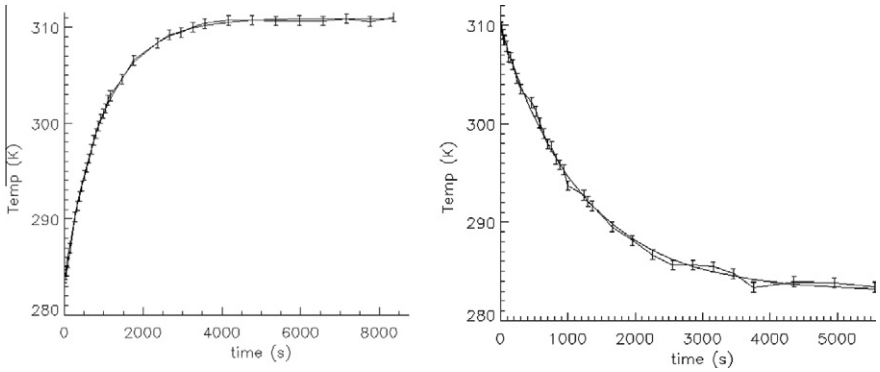

Fig. 14. CCR exponential heating (left) and cooling (right) curves with SS turned on and turned off: $\tau_{CCR} = (1100 \pm 100)$ s, $\Delta T = (28 \pm 1)$ K.

Please cite this article in press as: Dell'Agnello, S., et al. Creation of the new industry-standard space test of laser retroreflectors for the GNSS and LAGEOS. J. Adv. Space Res. (2010), doi:10.1016/j.asr.2010.10.022

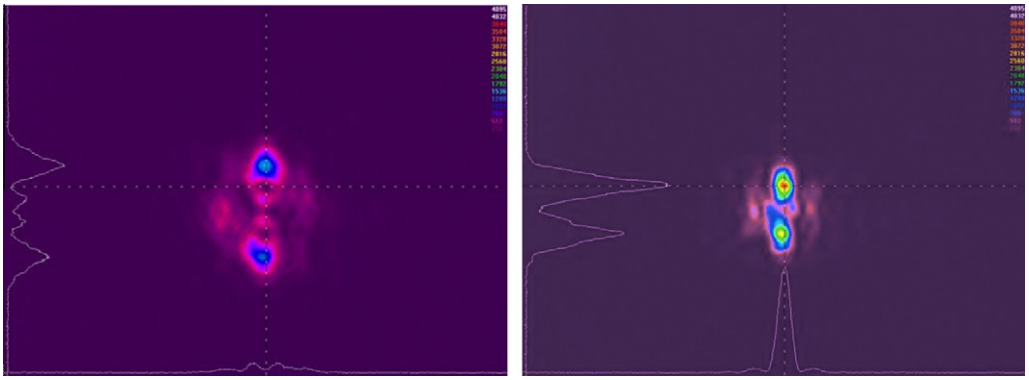

Fig. 15. SCF-Test of the GLONASS CCR prototype: hot (left) and cold (right) FFDPs taken at the end of the curves shown in Fig. 14.

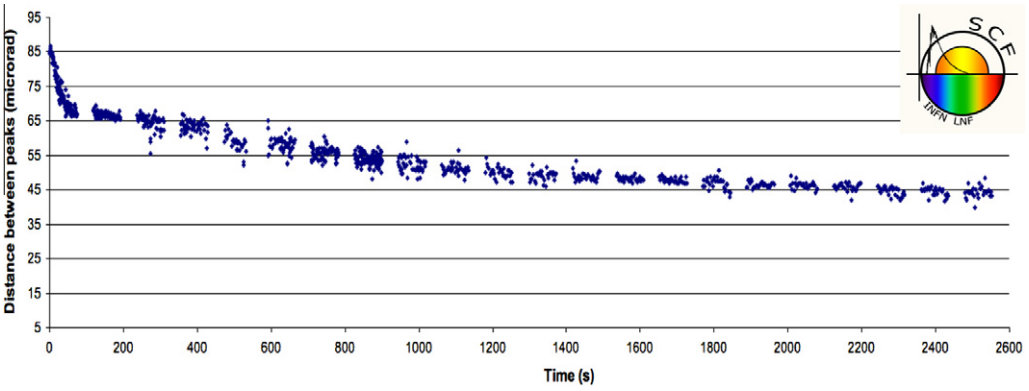

Fig. 16. Distance between peaks vs. time during GLONASS/GIOVE CCR cooldown.

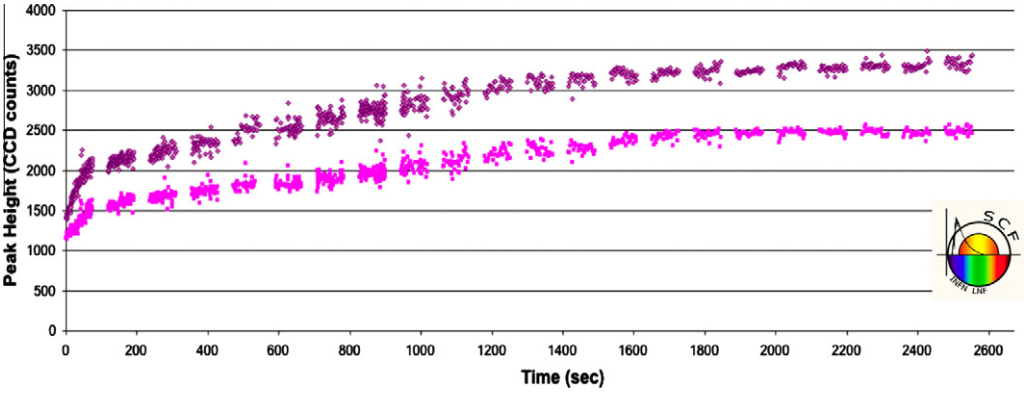

Fig. 17. GLONASS/GIOVE CCR cool-down: FFDP peak intensities vs. time.

from the bulk of the cube corner. This is distributed through the CCR so the average path length is shorter and the gradient due to this heat source is lower. When the SS is turned off, the solar heating of the thin metallic coatings stops. The gradient due to this heat source disappears in a few minutes since this process occurs by conduction. The remaining heat source is the bulk of the cube corner. Turning off the SS changes the equilibrium temperature. The cube corner starts to cool down with a long time constant because this is a radiative process, which is slower than conductive heat transfer. As the cube corner cools the amount of heat radiated from the front face decreases and the gradient decreases. This is aggravated by a slow thermal stabilization of the complex mounting components inside the CCR cavity. Here the heat flows through multiple interfaces between the components and the metallic coated back faces of the CCR. This effect is absent in the Apollo/LAGEOS CCR mounting scheme.

The actual FFDP thermal degradation was worse than the factor of two shown in Fig. 17. In fact, ILRS stations tracking GNSS satellites are located in the FFDP plane at a fixed velocity aberration of about 25 μrad. Therefore, if the peak of the energy return decreases AND it also moves away from this region, ILRS stations only detect the tail of a smaller peak. Fig. 18 shows the maximum of the FFDP intensity that we measured during the SCF-Test

Please cite this article in press as: Dell'Agnello, S., et al. Creation of the new industry-standard space test of laser retroreflectors for the GNSS and LAGEOS. J. Adv. Space Res. (2010), doi:10.1016/j.asr.2010.10.022

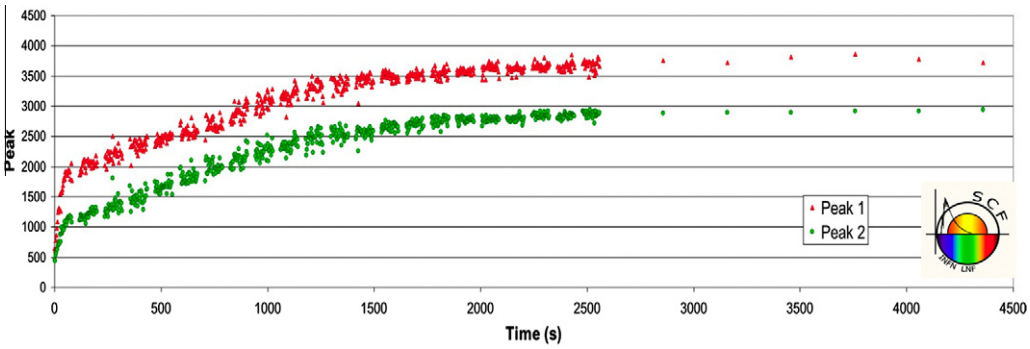

Fig. 18. GLONASS/GIOVE CCR cool-down: FFDP intensity at the average velocity aberration of ILRS stations for GNSS satellites (25 μrad) vs. time.

in this region of fixed velocity aberration, on the tail of the two peaks. Compared to the asymptotic, unperturbed value, the FFDP return energy is degraded (reduced) by the average multiplicative factor 0.14 ± 0.02 (14%). The uncertainty is given by the different reduction of the peaks and by statistics. A 1-m receiving telescope of an ILRS station is equivalent to ~1 pixel on the FFDP of our CCDs.

The results of this very first SCF-Test clearly show the significant capabilities of this new tool for the characterization of CCR FFDPs in laboratory-simulated space conditions. They also show that FFDP thermal degradations are a very large effect (0.14 ± 0.02) and that for future GNSS satellites it is wise to characterize LRAs during their development phase and in, any case, before launch. For the GNSS satellites already in orbit, SCF-Tests have been useful to explain experimentally their degraded behavior.

Note that this GLONASS CCR with standard polished Al housing was recently made, like the GLONASS-type reflectors deployed on GIOVE-A and -B in 2007/8. In the next section we show the SCF-Test of a very old GLONASS-type CCR built at the beginning of the 1990s for the GPS constellation. For this old flight CCR we find a marginally greater thermal degradation in the FFDP intensity (0.12 ± 0.02).

We point out that GLONASS/GIOVE/GPS LRAs are illuminated by the sun at an angle with respect to the normal to the LRA plane, which varies from 0° to 90° (when this angle is between 0° and −90° the spacecraft shades the LRA from the sun). This induces changes in the thermal perturbations. Instead of the SCF-Tests reported above, SS illumination angles different from 0° can be used. LRAs can also be rotated about the vertical in real time to simulate conditions in some segments of the orbit. This was done successfully for ESA for a Galileo IOV prototype CCR (see Section 7).

6. Test of the 1990s GPS flight model coated retroreflector array

6.1. FFDP tests in air and isothermal conditions at 632 and 532 nm

We performed individual FFDP tests on each of the 32 CCRs in the array in air and in isothermal conditions at 632 and 532 nm laser wavelengths in the SCF with the laser beam at normal incidence. Fig. 19 shows the FFDPs of three CCRs mounted with different relative orientations. FFDPs taken at 532 nm look more intense because the CCD shutter time used at the 532 nm was shorter that at 632 nm. This shorter shutter time was the same used to acquire reference Airy patterns. At 632 nm, the two peaks for 13 of the CCRs were merged into one (see the rightmost picture in Fig. 19). In some cases, thermal perturbations might separate these into two peaks. This can be inferred by the GLONASS SCF-Test reported in the previous section, which showed that after the SS heating the FFDP peaks were moved to higher order diffraction rings of the pattern; similarly the central peak energy would be transferred by thermal perturbations to the first diffraction rings, at the nominal, correct value of the velocity aberration.

Fig. 20 shows the peak-to-peak distance for the 25 CCRs, which have two clean separated peaks either at 632 nm or at 532 nm. This distance is consistent with the GNSS velocity aberration, ~25 μrad, within the measurement uncertainty of 5–10 μrad, including statistical and systematic errors. We expect to improve our estimate of this error as new funding becomes available for better hardware. Six CCRs have separate peaks only at 532 nm. Four have separate peaks only at 632 nm. The full set of measured patterns of this flight LRA shows a very wide variation of shape and intensity.

6.2. Optical cross sections: calculations, measurements and ILRS standard

The amount of information contained in the measured patterns is greater than that reported in Fig. 20. The FFDPs can be used to compute the incoherent (*inc*) optical cross section, σ, of the whole GPS flight LRA in AIC, for normal incidence of the laser beam ("on-axis"), $\sigma_{GPS,inc,AIC,0}$. The optical cross section is an intrinsic characteristic of CCRs and LRAs (Degnan, 1993). The optical cross section of a laser retroreflector array is given in square meters and can be thought of as the size of a diffusely reflecting board in space that gives the same reflected signal strength as the retroreflector array. The retroreflectors return large signals with small reflecting

Please cite this article in press as: Dell'Agnello, S., et al. Creation of the new industry-standard space test of laser retroreflectors for the GNSS and LAGEOS. J. Adv. Space Res. (2010), doi:10.1016/j.asr.2010.10.022

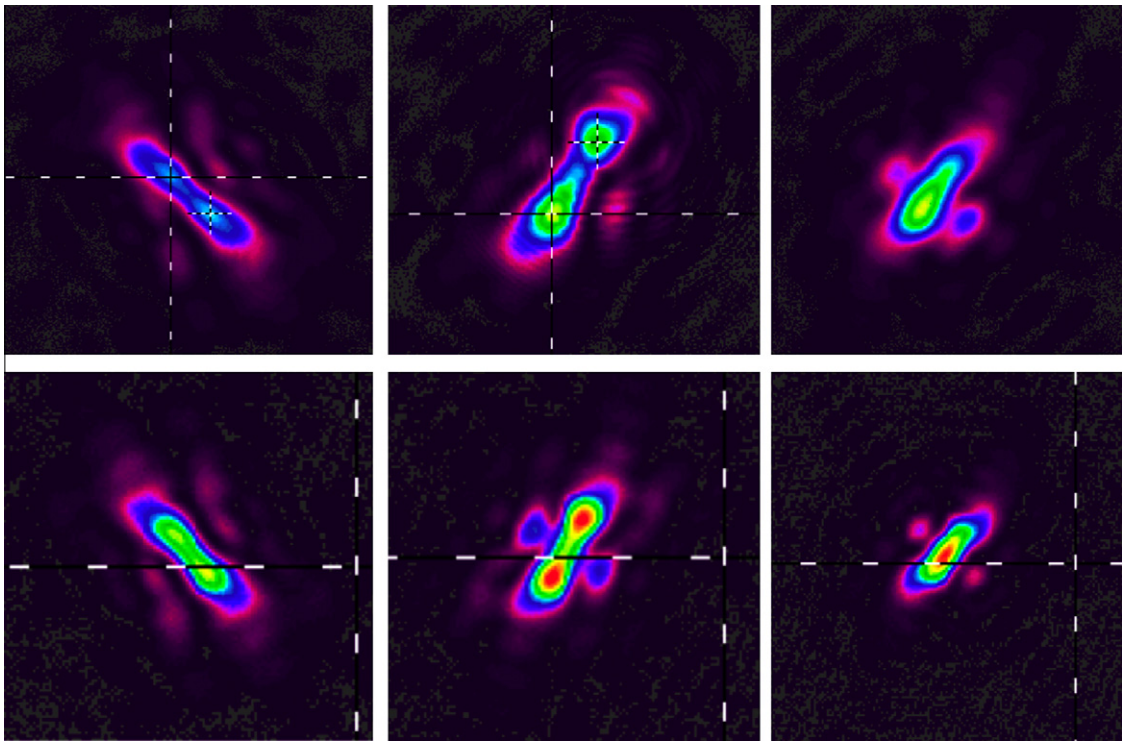

Fig. 19. FFDPs of GPS flight model retroreflectors in air, $T = 295$ K, taken at 632 nm (top three) and at 532 nm (bottom three).

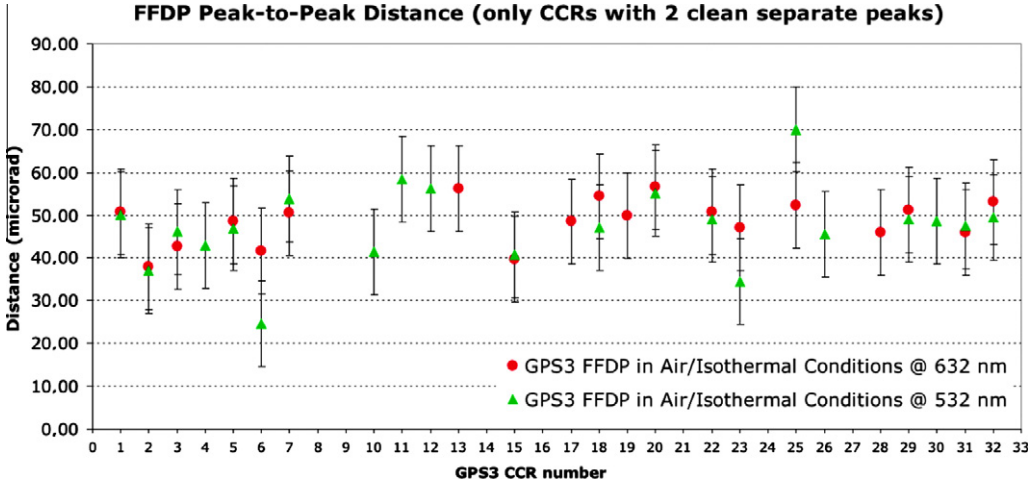

Fig. 20. FFDPs of the GPS flight retroreflectors with two clean separate peaks taken at 632 and 532 nm in air and isothermal conditions. The nominal distance is ~50 μrad.

areas because of their large optical signal the gain, which is the degree of angular concentration of the reflected beam. The cross section can be defined as the reflecting area times the gain. The cross section at the center of the diffraction pattern of a circular aperture is $4\pi\ (A/\lambda)^2$ in standard units, where A is the area of the circle and λ is the wavelength.

We computed our measured on-axis effective cross section of the GPS flight LRA as the incoherent sum of the 32 FFDPs as a function of the θ_x and θ_y angles in the FFDP (velocity aberration) plane, using the formula:

$$\sigma_{\mathrm{GPS},inc,\mathrm{AIC},0}(\theta_x,\theta_y) = \sigma_{\mathrm{AP,AIC},0} \times \sum_{i=1,32} \mathrm{FFDP}_{\mathrm{CCR}(i)}(\theta_x,\theta_y) \Big/ \mathrm{FFDP}_{\mathrm{AP}}(\theta_x = 0, \theta_y = 0),$$

where:

- $\sigma_{\mathrm{AP,AIC},0} = 4\pi\ (\mathrm{A}_{\mathrm{CCR}}\lambda)^2$ is the Airy Peak, on-axis, optical cross section of a perfect mirror with unit reflectivity and circular area A_{CCR} equal to that of the CCR.
- $\mathrm{FFDP}_{\mathrm{AP}}(\theta_x = 0, \theta_y = 0)$ is the measured intensity of that Airy Peak in CCD counts.

Please cite this article in press as: Dell'Agnello, S., et al. Creation of the new industry-standard space test of laser retroreflectors for the GNSS and LAGEOS. J. Adv. Space Res. (2010), doi:10.1016/j.asr.2010.10.022

- $FFDP_{CCR(i)}(\theta_x, \theta_y)$ is the measured intensity of the CCR pattern in the CCD counts.

$\sigma_{GPS,inc,AIC,0}(\theta_x, \theta_y)$ and its average around a circle of increasing velocity aberration (defined as $(\theta_x^2 + \theta_y^2)^{1/2}$) are shown in Figs. 21 and 22 for $\lambda = 632$ nm and $\lambda = 532$ nm, respectively. The cross section vs. velocity aberration at 632 nm is steeper than at 532 nm. Also shown in Figs. 21 and 22 are $\sigma_{GPS,inc,AIC,0}$ at three fixed values of velocity aberration vs. the azimuth in the θ_x, θ_y plane. Based on measurement checks and optical modeling with CODE V, we estimate a relative uncertainty on $\sigma_{GPS,inc,AIC,0}(\theta_x, \theta_y)$ of 20%, dominated by the finite optical quality of the FFDP circuit and our optical modeling. We expect to decrease this uncertainty as new funding becomes available for better hardware. At 25 μrad, our measured $\sigma_{GPS,inc,AIC,0}$ at $\lambda = 632$ nm and $\lambda = 532$ nm are (10.1 ± 2.0) million m^2 and (16.4 ± 3.3) million m^2, respectively. For $\lambda = 532$ nm this corresponds to a factor 6 reduction compared to the ILRS Retroreflector standard for GPS altitudes. The results obtained for 532 nm are summarized in Table 1. The LRA cross sections calculated by D. Arnold for GNSS satellites whose CCRs were measured at the SCF are shown in Table 1, together with the cross sections required by ILRS, the GPS flight LRA cross section measured in air and the results of the SCF-Tests reported in Sections 5.2 and 6.3. The latter results, shown in the last column of Table 1, indicate how much the in-air FFDP intensity (and therefore, the cross sec-

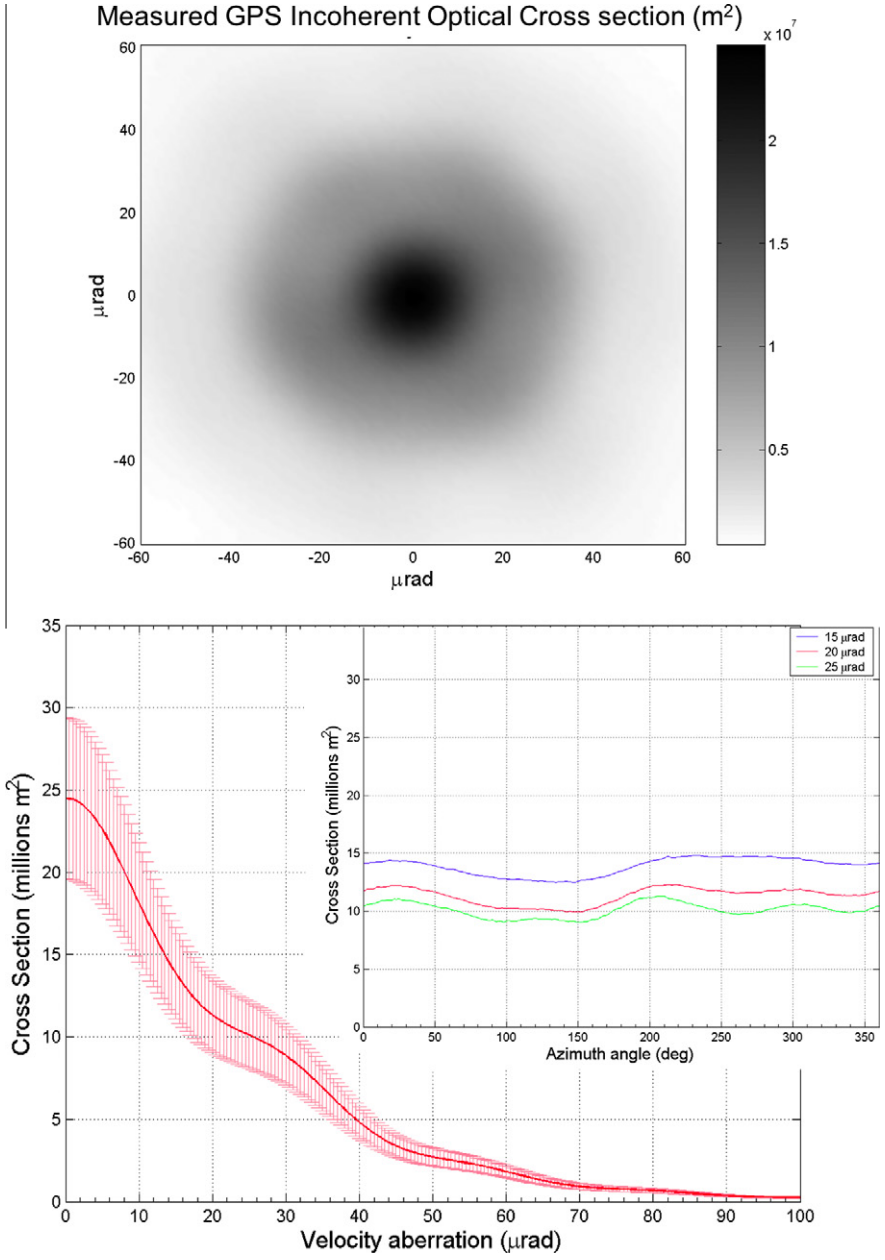

Fig. 21. GPS incoherent on-axis optical cross section measured at 632 nm. Top plot: $\sigma_{GPS,inc,AIC,0}$ vs. θ_x, θ_y. Bottom plot: averaged $\sigma_{GPS,inc,AIC,0}$ vs. velocity aberration; inset: $\sigma_{GPS,inc,AIC,0}$ vs. azimuth counted anticlockwise from the $\theta_x > 0$ axis of the top plot.

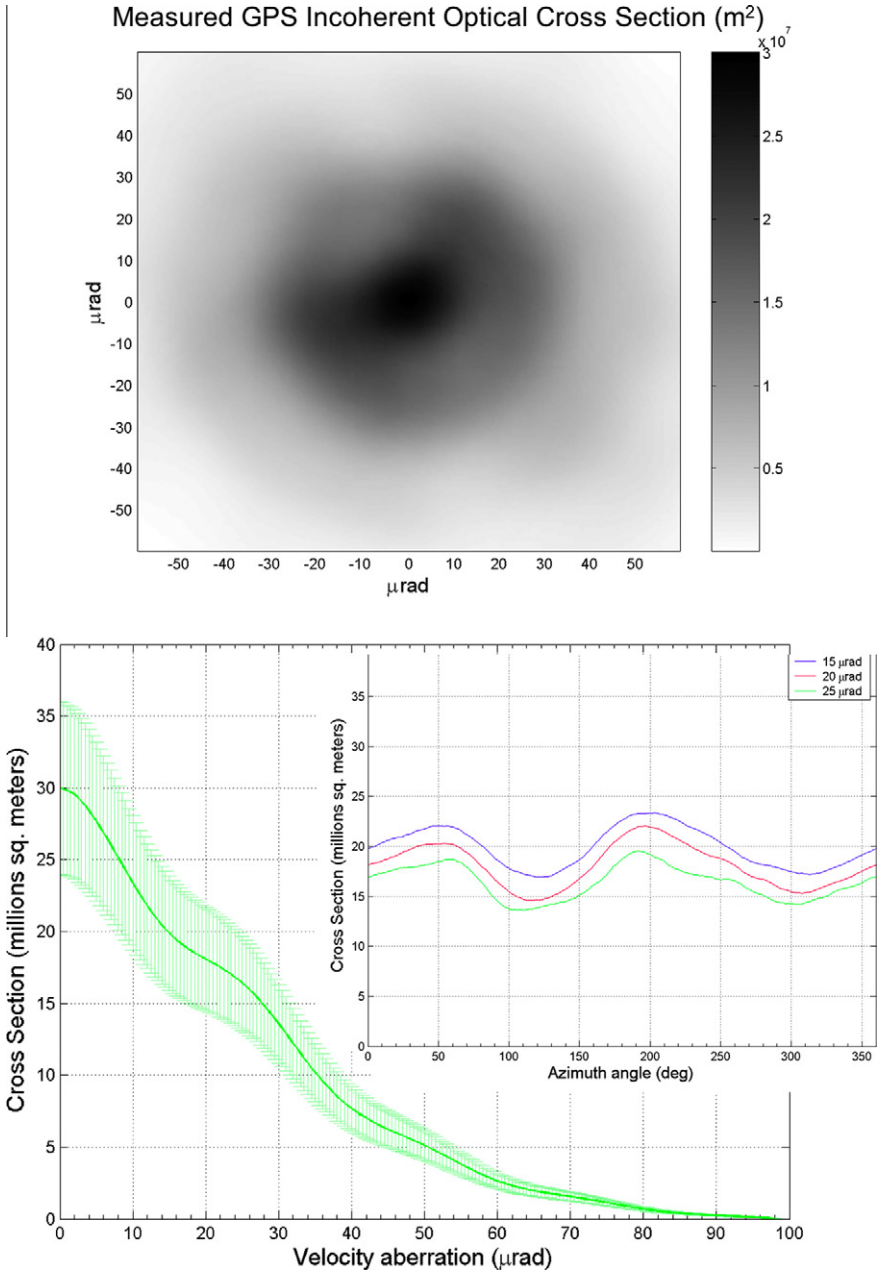

Fig. 22. GPS incoherent on-axis optical cross section measured at 532 nm. Top plot: $\sigma_{GPS,inc,AIC,0}$ vs. θ_x, θ_y. Bottom plot: averaged $\sigma_{GPS,inc,AIC,0}$ vs. velocity aberration; inset: $\sigma_{GPS,inc,AIC,0}$ vs. azimuth counted anticlockwise from the $\theta_x > 0$ axis of the top plot.

tion) is degraded due to thermal effects in the specific configuration of our SCF-Tests. Exposure to the full AM0 intensity and IR spectrum could give different thermal degradations. In future tests we will compensate these limitations (IR cutoff at 3 μm and slightly reduced solar constant), which were imposed by funding constraints.

6.3. SCF-Test of one retroreflector of the GPS flight model array at 532 nm

We performed the SCF-Test of four CCRs at 532 nm laser wavelength. The measurement and analysis followed the flow described for the GLONASS above. The bulk temperature of the third GPS flight array was controlled with a custom copper plate in thermal contact with the Al base plate of the array using indium washers. The copper plate was in turn thermally controlled with a fluid driven by an external chiller. The temperature of the Al back plate of the array was measured with a PT100 probe; during the test it was set to (292 ± 1) K. The solar constant had a slightly reduced value of $(0.89 \pm 0.05) \times$ AM0 due to aging of the lamps. We present the FFDP variations vs. time for one of the GPS CCRs. The temperature variations of the CCR front face, with its hottest and coldest FFDPs are shown in Fig. 23.

The FFDP behavior vs. time is shown in Fig. 24. The oscillation of the FFDP peak heights shown in Fig. 24 (bottom) for times above 2000 s is due to an instability of

Please cite this article in press as: Dell'Agnello, S., et al. Creation of the new industry-standard space test of laser retroreflectors for the GNSS and LAGEOS. J. Adv. Space Res. (2010), doi:10.1016/j.asr.2010.10.022

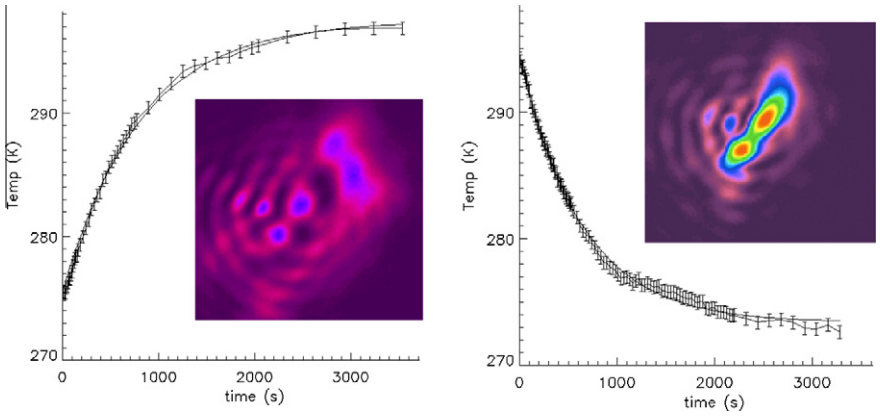

Fig. 23. Warm-up (left), cool-down (right) curves of the CCR front face and FFDPs taken at the end of the curves. Exponential fits give $\tau_{CCR} = (720 \pm 80)$ s, $\Delta T = (21.5 \pm 0.6)$ K.

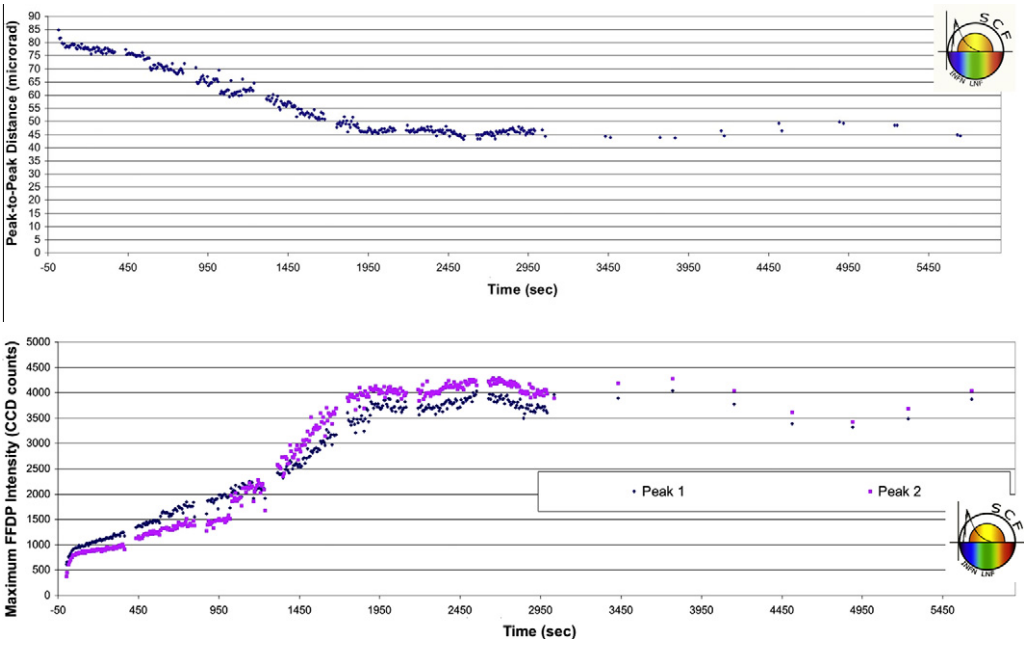

Fig. 24. GPS CCR cool-down: FFDP peak distance vs. time (top); maximum FFDP intensities at the average GNSS velocity aberration (25 μrad) vs. time (bottom).

a few degrees in our thermal control system. This technical issue was imposed during the test activity by funding limitations. This effect shows that systematic LRA bulk temperature changes directly influence the LRA optical performance.

This data shows that the optical performance is significantly degraded for this geometric and thermal configuration. The FFDP peaks are disrupted and scattered all over the CCD. For the first 10–20 s the peaks cannot be defined. The fast decrease/increase of the peak distance/height that is clearly visible for the 2007 GLONASS CCR is less clear for this CCR. The degradation of the initial "hot" FFDP is worse probably because the GPS flight LRA is older (early 1990s) and less optimized. However, the reduction in intensity between the hot and cold conditions at 25 μrad is a factor of 0.12 ± 0.02, slightly lower than for the 2007 GLONASS/GIOVE CCR.

In summary, for a velocity aberration of 25 μrad we measured an incoherent, isothermal optical cross section a factor ~6 lower than the ILRS standard. In our SCF-Test with on-axis SS illumination, $0.89 \times$ AM0 and IR < 3 μm, FFDP thermal degradations were 0.12 ± 0.02. The 0.02 uncertainty is estimated by differences in the reduction of the peaks and by statistics. In our specific test, this amounts to a factor ~50 reduction (~$6 \times 1/0.12$) of the effective space cross section compared to the ILRS requirement.

SCF-Tests will help predict the SLR return signal strength from the GNSS CCRs before launch. This will require modeling to correct the data for residual differences

Please cite this article in press as: Dell'Agnello, S., et al. Creation of the new industry-standard space test of laser retroreflectors for the GNSS and LAGEOS. J. Adv. Space Res. (2010), doi:10.1016/j.asr.2010.10.022

between SCF and orbital configurations. The ILRS requirement for its optical cross section for Galileo at 23,200 km altitude is 180 million m^2. Therefore, greater care must be taken to make the return pattern uniform when the satellite moves across the sky and to avoid degradations due to thermal effects. Our ultimate goal is to optimize the LRA design, boost and smooth-out the signal strength to allow for daylight ranging by the majority of ILRS stations (unlike now).

7. Uncoated retroreflectors for modern GNSS

Uncoated retroreflectors are emerging as the recommended design for modern GNSS satellites. They were adopted by the Chinese COMPASS-M1 and by the Russian GLONASS-115, launched in 2009. These two satellites give better SLR signal strength than older GNSS LRAs with coated CCRs, as shown by Fig. 25. GLONASS-115 maintains the old GLONASS, GPS, GIOVE and IOV LRA design with single-CCR cavities mounted on a separate plate, but is the first of its constellation with uncoated cubes. No COMPASS or uncoated GLONASS CCR has been available for SCF-Testing.

Critical LRA design elements that help the optimization process for modern GNSS include (Pearlman, 2009; Arnold et al., 2009; Dell'Agnello, 2009; see also http://www.ntua.gr/MIRC/ILRS_W2009/):

- Uncoated cubes in an LRA designed to minimize thermal degradations of σ, with a thermally insulated mounting scheme is very important: (Apollo *docet*, LAGEOS confirms) which tested in laboratory-simulated space conditions.
- Zero dihedral angle offset with a tolerance no larger than 0.5″ and cube diameter chosen in order to place the first FFDP diffraction ring at the relevant velocity aberration for GNSS altitudes. The zero angle avoids polarization effects in the intensity of the FFDP.
- Sets of 4 cubes oriented at 0°, 30°, 60°, and 90° in azimuth; this clocking is needed to produce a smooth first ring in the intensity of the diffraction pattern.

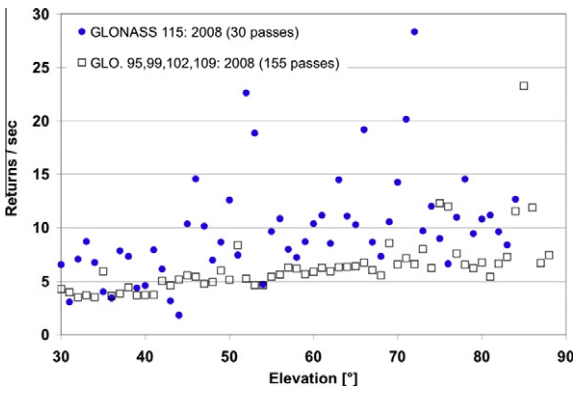

Fig. 25. Laser returns/s by old Al-coated LRAs (GLONASS 95, 99, 102, 109) and the recently launched uncoated GLONASS-155 LRA.

- Each set of 4 cubes with the same orientation symmetrically placed so their centroids are approximately at the center of the array to avoid range biases.
- Approximately circular shape of the array (for example hexagonal) to minimize variations on range spread as the array is viewed from different directions.
- Well-documented 'as-built' LRA performance SCF-Tests prior to launch under environmental conditions similar to those anticipated on the spacecraft in orbit.

An uncoated Galileo IOV prototype cube was SCF-Tested at LNF by the ETRUSCO INFN experiment for ESA. Two KPIs were characterized during several SCF-Tests; the measurements delivered to ESA included: (1) τ_{CCR} for T_M varied over a very large temperature range and (2) FFDPs with the experimental simulation of a specific and critical satellite orbit, potentially subject to large thermal degradations of the FFDP. For KPI (2) we changed the orientation the CCR in real-time and recorded its FFDP while the SS was illuminating the CCR to simulate conditions of sunrise (3 h), sun eclipse due to Earth shadow (1 h) and sunset (3 h) over the CCR. This was equivalent to half of a specific Galileo orbit. This included the so-called *breakthrough* of the SS light (and heat) inside the IOV CCR cavity due to loss of total internal reflection for certain SS illumination angles. The results, intellectual property of INFN and subject to a non-disclosure agreement between INFN-LNF and ESA (ESA reference RES-PN/CH/ch10.148), will be reported when ESA will give its authorization. Further and extensive SCF-Testing is needed to fully assess the performance of IOV LRAs for the benefit of orbit data analysis and future array design and optimization.

Finally, we report one result out of several SCF-Tests on the LAGEOS "Sector" engineering model (see Boni et al., 2008) owned by NASA-GSFC and built in the early 1990s. This LRA is relevant to show as a 'calibration' of the SCF-Test and apparatus because LAGEOS is the reference and standard SLR payload for ILRS and because the Apollo/LAGEOS CCR design and mounting scheme is the standard for LRA optimization and ranging performance.

The Sector: 380 mm diameter, weighing 15 kg, with 37 CCRs of good optical quality, was FFDP-tested at LNF with 632 and 532 nm laser wavelengths (Dell'Agnello, 2009). In the SCF, the Sector was thermally controlled with a custom copper plate attached to its back. Fig. 26 shows the FFDP intensity of the polar CCR at a velocity aberration of 35 μrad during a default SCF-Test ($T_{AVG} = 300$ K, 0° angle SS illumination, see Section 4), like those performed for the GLONASS/GIOVE prototype CCR and the GPS flight LRA. FFDP intensities are relative fractions of a reference FFDP taken in the SCF in approximately stationary conditions at the beginning of the test, at time = 0 s and with SS turned off. After the SS was on for 3 h, the Sector was rotated towards the laser window and the SS was simultaneously turned off. The FFDPs were then recorded for 3 h. The uncertainty on the data (±10%)

Please cite this article in press as: Dell'Agnello, S., et al. Creation of the new industry-standard space test of laser retroreflectors for the GNSS and LAGEOS. J. Adv. Space Res. (2010), doi:10.1016/j.asr.2010.10.022

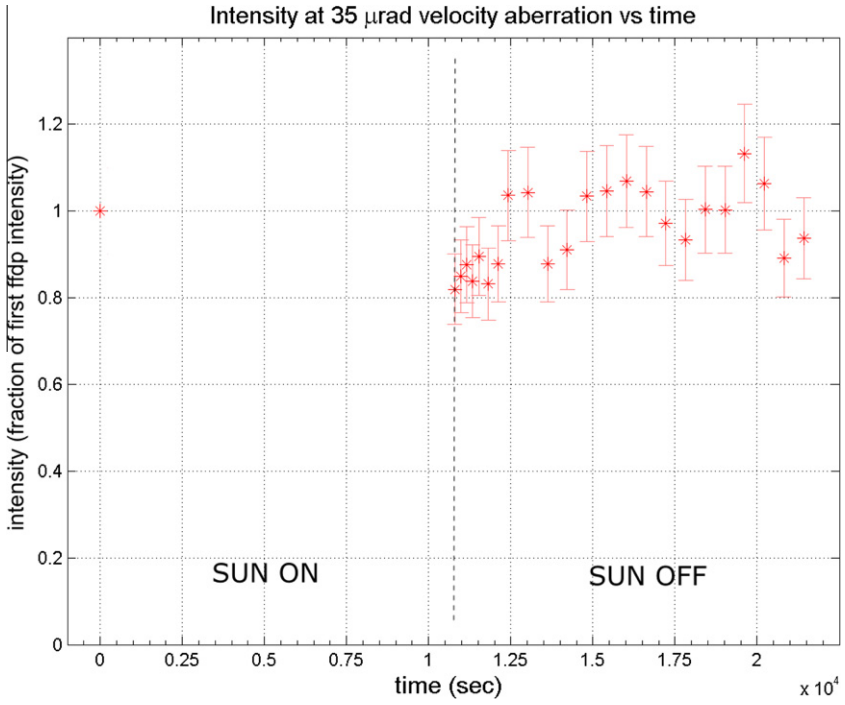

Fig. 26. Variation of LAGEOS FFDP relative intensity during a default SCF-Test with linear polarization of the interrogating laser. The reference 'first FFDP' is the one taken at time = 0 s just before turning on the SS for 3 h.

is due to FFDP count statistics and to systematic variations of the SCF conditions during the test.

As expected, the LAGEOS FFDP thermal degradation was significantly smaller than those we measured for GLONASS/GPS/GIOVE. Other SCF-Tests were conducted varying T_M, the SS illumination angle and the CCR mount conductance (by changing the torque of the screws holding the CCR in its mount).

Systematic τ_{CCR} measurements were made on many of the CCRs. The measured LAGEOS τ_{CCR} was significantly longer than those on the GLONASS/GPS/GIOVE CCRs, even after scaling the measured τ_{CCR}'s by the respective CCR masses. This confirms that the Apollo arrays and LAGEOS are more optimized and have lower CCR mount conductance than GLONASS/GPS/GIOVE satellites.

8. Conclusions

We have created a unique facility and a new industry-standard laboratory test to validate the thermal and optical behavior of laser retroreflectors in space for industrial and scientific applications. We identified SLR/LLR Key Performance Indicators (KPIs) and their associated deliverables to be characterized through the SCF-Test (τ_{CCR}, FFDP, OLP, WFI). The SCF and SCF-Test were developed in the context of the ETRUSCO experiment at INFN-LNF and are background intellectual property of INFN. The SCF-Test exploits modern hardware and software tools and novel ideas to respond to today's needs for increased accuracy and link signal strength. At the same time, it is also rooted in the experience of the ILRS and of the most successful LRA payloads, Apollo and LAGEOS.

We reported the results of the SCF-Test of a GPS flight model LRA and of a GLONASS/GIOVE prototype CCR. We found that in some space configurations they showed FFDP thermal degradations (reductions) of a factor eight and seven, respectively. We ascribe these degradations to the retroreflector metal coating and to the non-optimized thermal mount conductance of this old generation of retroreflectors.

Uncoated retroreflectors with minimum thermal degradation, which can be quantified and minimized with prelaunch SCF-Testing, are emerging as the recommended design for modern GNSS satellites. Keeping thermal degradations lower than for older generation coated retroreflectors will improve daylight ranging, thus helping the future combination of SLR and GNSS observations for precise orbit reconstruction, and thus allowing the ILRS to be able to track the increasing number of GNSS Constellations.

The IOV and LAGEOS measurements proved the effectiveness of the SCF-Test as an LRA diagnostic, optimization and validation tool in use by NASA, ESA and ASI. Therefore, we are going to propose the SCF-Test as a new industry-standard space test to be considered by the forthcoming releases of ESA's European Space Technology Master Plan. Further development of the SCF-Test is continuing with an ASI "Project of Technological Development" led by INFN as prime contractor (ASI-INFN Contract No. I/077/09/0), ETRUSCO-2. A kick-off meeting was held on May 11, 2010, and the project is due to be completed by mid 2013. The SCF-Test is also available

Please cite this article in press as: Dell'Agnello, S., et al. Creation of the new industry-standard space test of laser retroreflectors for the GNSS and LAGEOS. J. Adv. Space Res. (2010), doi:10.1016/j.asr.2010.10.022

to space agencies and industry and, in particular, for applications to GNSS constellations.

Acknowledgments

Very special thanks to E. Saggese (President of ASI, formerly at Finmeccanica), M. Bizzarri, M. Spagnulo, M. Cosmo and A. Tuozzi of ASI for encouraging and inspiring this work since its early conception. We thank Daniel Navarro-Reyes and Rafael Garcia Prieto of ESA-ESTEC for useful discussions on GIOVE and Galileo IOV satellites.

We then wish to thank V. Vasiliev of the IPIE of Moscow for making the GLONASS CCRs available for testing at the LNF facilities and J.J. Degnan for useful suggestions on laser ranging instrumentation.

We thank G. Giordano of INFN-LNF for allowing the use of the Optics Lab, which helped significantly the start-up of our work. We also thank M. Calvetti, C. Sanelli, U. Bottigli, B. D'Ettorre Piazzoli, A. Vacchi, G. Cuttone, S. Bertolucci, R. Battiston, V. Chiarella of the INFN and LNF Management, and R. Cimino, LNF representative of the National Technology Research Committee of INFN ("Commissione Scientifica Nazionale V"), for supporting and encouraging this research activity. The LNF Support Services (Cryogenics, Mechanics and Metrology, Electronics and Automation) also gave a significant help to this experimental program.

Appendix A. List of acronyms and definitions

AC	Analysis Center
AIC	Air and Isothermal Conditions
AM0	Air Mass zero
APOLLO	Apache Point Observatory Lunar Laser-ranging Operation
ASI	Agenzia Spaziale Italiana i.e. Italian Space Agency
CC	Combination Center
CCD	Charged Coupled Device
CCR	Cube Corner Retroreflector
CGS	Centro di Geodesia Spaziale i.e. Space Geodesy Center
DAO	Dihedral Angle Offset
DORIS	Doppler Orbitography and Radiopositioning Integrated by Satellite
ES	Earth infrared Simulator
ESTEC	European Space research and TEchnology Centre
ETRUSCO	Extra Terrestrial Ranging to Unified Satellite COnstellation
FEM	Finite Element Method
FFDP	Far Field Diffraction Pattern
GIOVE	Galileo In-Orbit Validation Element
GLONASS	GLObal NAvigation Satellite System
GNSS	Global Navigation Satellite System
GPS	Global Positioning System
GSFC	Goddard Space Flight Center
HMI	Hydrargyrum Medium-arc Iodide
IAG	International Association of Geodesy
IDS	International DORIS Service
IERS	International Earth rotation and Reference system Service
IGS	International GNSS Service
ILRS	International Laser Ranging Service
INFN	Istituto Nazionale di Fisica Nucleare
IOV	In Orbit Validation
IPIE	Institute of Precision Instrumentation Engineering
IR	Infra Red
ITRF	International Terrestrial Reference Frame
ITRS	International Terrestrial Reference System
IUGG	International Union of Geodesy and Geophysics
IVS	International VLBI Service
KPI	Key Performance Indicator
LAGEOS	LAser GEOdynamics Satellite
LNF	Laboratori Nazionali di Frascati
LRA	Laser Retroreflector Array
LLR	Lunar Laser Ranging
OLP	Orthogonal Laser Polarizations
O.R.A.	Optical Research Associates
PID	Proportional Integral Derivative
RMS	Root Mean Square
SCF	Satellite/lunar laser ranging Characterization Facility
SIP	Support and Interface Plate
SLR	Satellite Laser Ranging
SS	Solar Simulator
TEC	Thermo Electric Cooler
ToF	Time of Flight
TRS	Thermal Desktop RadCad Sinda-Fluint
UV	Ultra Violet
VLBI	Very Long Baseline Interferometry
WFI	Wavefront Fizeau Interferogram

References

Altamimi, Z., Collilieux, X., Legrand, J., et al. ITRF2005, a new release of the International Terrestrial Reference Frame based on time series of station positions and Earth orientation parameters. J. Geophys. Res. 112 (B9), B09401, 2007.

Arnold, D.A. Uncoated cubes for GNSS satellites, in: International Technical Laser Workshop on SLR Tracking of GNSS Constellations, Metsovo, Greece, 2009.

Battat, J., Murphy, T.W., Adelberger, E.G., et al. The Apache Point Observatory Lunar Laser-ranging Operation (APOLLO): two years of millimeter-precision measurements of the earth–moon range. PASP 121 (875), 29–40, 2009.

Bender, P.L., Currie, D.G., Dicke, R.H., Eckhardt, D.H., Faller, J.E., Kaula, W.M., Mulholland, J.D., Plotkin, H.H., Poultney, S.K., Silverberg, E.C., Wilkinson, D.T., Williams, J.G., Alley, C.O. The lunar laser ranging experiment. Science 182 (4109), 229–238, 1973.

Please cite this article in press as: Dell'Agnello, S., et al. Creation of the new industry-standard space test of laser retroreflectors for the GNSS and LAGEOS. J. Adv. Space Res. (2010), doi:10.1016/j.asr.2010.10.022

Bian, S., Jin, J., Fang, Z. The Beidou satellite positioning system and its positioning accuracy. Navigation 52 (3), 123–130, 2005.

Boni, A., Cantone, C., Dell'Agnello, S., Delle Monache, G.O., Garattini, M., Intaglietta, N., Lops, C., Martini, M., Porcelli, L. Optical far field diffraction pattern test of laser retroreflectors for space applications in air and isothermal conditions at INFN-LNF. INFN-LNF Report LNF-08/26(IR), 2008.

Bosco, A., Cantone, C., Dell'Agnello, S., Delle Monache, G.O., et al. Probing gravity in NEOs with high-accuracy laser-ranged test masses. Int. J. Mod. Phys. D 16 (12A), 2271–2285, 2007.

Degnan, J.J. Millimeter Accuracy Satellite Laser Ranging: A Review, Contribution of Space Geodesy to Geodynamics: Technology Geodynamics Series, vol. 25, AGU Washington, 1993.

Dell'Agnello, S., Currie, D.G., Delle Monache, G.O., Murphy, T.W., et al. A lunar laser ranging retroreflector array for NASA's manned landings, the international lunar network and the proposed ASI lunar mission MAGIA, in: 16th International Workshop on Laser Ranging, Poznan, Poland, 2008.

Dell'Agnello, S., Delle Monache, G.O., Currie, D.G., Vittori, R., et al. SCF-Test of laser retroreflector arrays for next GNSS constellations, in: International Technical Laser Workshop on SLR Tracking of GNSS Constellations, Metsovo, Greece, 2009.

Dick, W.R., Richter, B. The International Earth Rotation and Reference Systems Service (IERS), in: Heck, André (Ed.), Organizations and Strategies in Astronomy (Astrophysics and Space Science Library, 310), vol. 5. Kluwer Academic Publishers Dordrecht, Boston, London, pp. 159–168, 2004.

Dow, J.M., Neilan, R.E., Rizos, C. The International GNSS service in a changing landscape of global navigation satellite systems. J. Geod. 83, 191–198, doi:10.1007/s00190-008-0300-3, 2009.

Falcone, M., Navarro-Reyes, D., Hahn, J., Otten, M., Piriz, R., Pearlman, M.R. GIOVE's Track. GPS World, 34, 2006.

Fumin, Y., Wanzhen, C., Yuanming, W., Pu, L. Laser retroreflector arrays on the COMPASS satellites, in: Proceedings of the 16th International Workshop on Laser Ranging, Poznan, Poland, 2008.

Geodesist's Handbook, Bulletin Geodesique, vol. 66, Springer-Verlag Berlin, 1992.

Pearlman, M.R., Degnan, J.J., Bosworth, J.M. The international laser ranging service. Adv. Space Res. 30 (2), 135–143, doi:10.1016/S0273-1177(02)00277-6, 2002.

Pearlman, M.R., Technological challenges of SLR tracking of GNSS constellations, in: International Technical Laser Workshop on SLR Tracking of GNSS Constellations, Metsovo, Greece, 2009.

Plag, H.-P., Pearlman, M.R. (Eds.), The Global Geodetic Observing System: Meeting the Requirements of a Global Society on a Changing Planet in 2020, Springer Berlin Heidelberg, 2009.

Schlüter, W., Behrend, D. The International VLBI Service for geodesy and astrometry (IVS): current capabilities and future prospects. J. Geod. 81, 379–387, doi:10.1007/s00190-006-0131-z, 2007.

Weber, R., Springer, T.A. The international GLONASS experiment, products, progress and prospects. J. Geod. 75 (11), 559–568, 2001.

Williams, J.G., Turyshev, S.G., Boggs, D.H., Ratcliff, J.T. Lunar laser ranging science: gravitational physics and lunar interior and geodesy. Adv. Space Res. 37 (1), 67–71, 2006.

Willis, P., Beutler, G., Gurtner, W., et al. IGEX, international GLONASS experiment scientific objectives and preparation. Adv. Space Res. 23 (4), 659–663, 1999.

Willis, P., Fagard, H., Ferrage, P. The international DORIS service (IDS): toward maturity. Adv. Space Res. 45, 1408–1420, 2010.

Please cite this article in press as: Dell'Agnello, S., et al. Creation of the new industry-standard space test of laser retroreflectors for the GNSS and LAGEOS. J. Adv. Space Res. (2010), doi:10.1016/j.asr.2010.10.022